communications biology

A Nature Portfolio journal

Article

https://doi.org/10.1038/s42003-025-08196-4

Changes in the assembly and functional adaptation of endophytic microbial communities in *Amorphophallus* species with different levels of resistance to necrotrophic bacterial pathogen stress

Min Yang, Ying Qi, Penghua Gao, Lifang Li, Jianwei Guo, Yongteng Zhao, Jiani Liu, Zebin Chen & Lei Yu

Pcc is one of the key pathogenic factors responsible for destructive soft rot in konjac. To date, the assembly and functional adaptation of the plant endophytic microbiome under *Pcc* stress remain poorly understood. Here, we found that *Pcc* stress leads to rapid reorganization of the endogenous microbiome in multiple organs of both susceptible and resistant konjac plants. Under *Pcc* stress, the negative interactions within the bacterial-fungal interdomain network intensified, suggesting an increase in ecological competition between bacterial and fungal taxa. We further discovered that the relative abundance dynamics of the classes Dothideomycetes and Sordariomycetes, as core fungal taxa, changed in response to *Pcc* stress. By isolating culturable microorganisms, we demonstrated that 46 fungal strains strongly inhibited the growth of *Pcc*. This implies that endophytic fungal taxa in konjac may protect the host plant through ecological competition or by inhibiting the growth of pathogenic bacteria. Metagenomic analysis demonstrated that microbial communities associated with resistant *Amorphophallus muelleri* exhibited unique advantages over susceptible *Amorphophallus konjac* in enhancing environmental adaptability, regulating plant immune signaling, strengthening cell walls, and inducing defense responses. Our work provides important evidence that endophytic fungal taxa play a key role in the host plant's defense against necrotizing bacterial pathogens.

Konjac (*Amorphophallus* spp.) plants are crucial economic crops for the food, chemical and pharmaceutical industries and can accumulate large amounts of glucomannan (KGM). However, bacterial soft rot caused by *Pectobacterium* spp., *Erwinia*, and *Dickeya* spp. is a widespread and catastrophic disease that poses a serious threat to konjac production[1]. This disease is often referred to as the 'cancer' of konjac, as it can result in yield losses of 30–70% or even complete crop failure[2,3]. *Pectobacterium* spp. are plant necrotic bacterial pathogens that can cause very destructive plant diseases, including common soft rot, blackleg, and stem wilt[4,5]. Infections caused by *Pectobacterium* spp. lead to severe losses in the cultivation of various field crops, vegetables, fruits and ornamental plants worldwide, and these pathogens are considered among the ten most dangerous plant pathogens[6–8]. *Pectobacterium carotovorum* subsp. *carotovorum* (*Pcc*) is one of the most destructive bacterial pathogens of *Amorphophallus konjac*. The main determinants of *P. carotovorum* pathogenicity are a series of extracellular pectinases. The type III secretion system of *Pcc* can produce various bacteriocins, including low-molecular-weight bacteriocins such as carocin (S1, S2, S3 and D), peccin (P, M1, and M2) and carotovorocin (a high-molecular-weight phage-like bacteriocin with unique properties), increasing their competitiveness with other relevant competitor species[9,10]. *Pcc* can infect all parts of the *A. konjac* plant (leaves, petioles, roots and tubers). This pathogen has a short disease cycle, leading to the rapid development of

College of Agronomy, Yunnan Key Laboratory of Konjac Biology, Yunnan Urban Agricultural Engineering and Technological Research Center, Kunming University, Kunming, 650214, China. e-mail: yulei0425@163.com

symptoms and rapid plant necrosis and rot. Under artificial inoculation stress, *A. konjac* shows obvious disease symptoms in a very short period (only 96 h), exhibiting petiole tissue collapse and lodging (Fig. 1a–e). Thus far, no study has focused on the relevant changes in the community composition and function of the endophytic microbiome in a relatively short period under necrotic bacterial pathogenic stress.

Plants provide many niches for the growth and proliferation of various microorganisms, including bacteria, fungi, protists, nematodes, and viruses (plant microbiota)[11,12]. Plants and associated microbial communities have coevolved for more than 400 million years. The interactions between plants and microbial communities are important for promoting the productivity and health of plants in natural environments[13–17]. Recent studies have demonstrated that the assembly of the plant microbiome and the health of the host are strongly affected by complex dynamic interactions among the host, microbes, and environment[18]. On the one hand, infection by pathogens and parasites often leads to changes in the structure and function of plant-associated microbial communities[19,20]. Pathogens and parasites may negatively affect host plant health by producing toxins, suppressing plant innate immunity and promoting the survival and reproduction of other plant pathogens and pests[21–24]. On the other hand, plants recruit a stress-related microbiota that provides protection against various abiotic and biotic stresses[25–28]. Therefore, the regulation of the plant microbiota is increasingly considered an environmentally sustainable method for protecting plants from diseases and promoting agricultural production[11,29]. To date, the basic ecological assembly patterns, co-occurrence patterns and functions of plant-associated microbial communities under pathogen stress are still poorly understood. A better understanding of the mechanisms by which plant hosts regulate their microbial communities and the functions of related microbial communities under pathogen stress is important for using plant microbial communities to improve plant health and maximize crop yield.

Plant-associated microbial communities include microorganisms associated with the rhizosphere (plant–root–soil interface), phyllosphere (air–plant interface) and inner sphere (internal tissues of plants)[30]. To date, most relevant studies have focused on the microbial communities in the rhizosphere and phyllosphere, while a systematic understanding of the structures and functions of the inner plant microbial communities under pathogen invasion is still lacking[31–35]. Studies on chili pepper[36], tomato[37], tobacco[38] and beet[39] have shown that the endophytic microbiomes of plants infected by pathogens can attract beneficial microbes to rescue and protect offspring (i.e., the "cry for help" strategy). However, these studies have focused mostly on *Fusarium* wilt and root rot caused by fungal pathogen infection. Although these diseases severely harm plant health, they are characterized by the gradual development of symptoms, slow progression of the disease, and slow rates of plant withering and death. Therefore, during infection by these fungal pathogens, the endophytic microbiomes of plants usually require a long period to recruit or reorganize in response to stress, and the changes in the endophytic microbial communities are not surprising. The assembly and functional adaptations of the endophytic microbiota under infection by bacterial pathogens, in addition to fungal pathogens, are poorly understood[40].

In this study, we hypothesize that the endophytic microbiota of konjac responds in a very short time under *Pcc* stress by recruiting protective microbes to inhibit the growth of pathogens. Furthermore, considering that

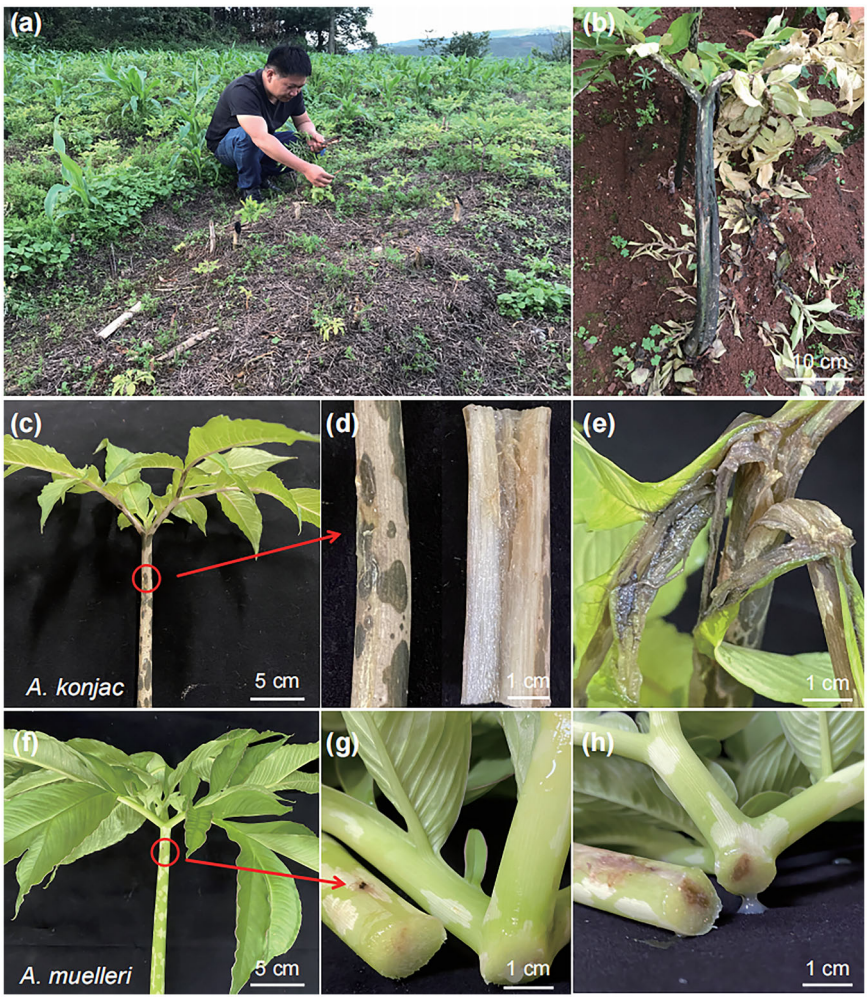

Fig. 1 | Symptoms of *A. konjac* (susceptible) and *A. muelleri* (resistant) plants infected with *Pcc*. **a** The mean incidence rate of bacterial soft rot in the field was greater than 35%. **b** Typical field symptoms of bacterial soft rot caused by *A. konjac*. **c** *A. konjac* (susceptible) plants injected with *Pcc*. **d** At 48 h post infection (hpi), thick liquid flowed out from the inoculation point, and the internal tissue of the *A. konjac* petiole began to show water-soaked rot. **e** At 96 hpi, the internal tissue of the *A. konjac* petiole had rotted, turned black over a large area and become watery, leading to lodging symptoms in the whole plant. **f** *A. muelleri* (resistant) plants injected with *Pcc*. **g** At 48 hpi, only slight browning of the internal tissue of the *A. muelleri* petiole was observed. **h** At 96 hpi, the tissue near the inoculation site on the petiole presented brown lesions, but no signs of petiole tissue rot or lodging were observed.

the selective enrichment of the stress-tolerant microbiota is driven by differences in plant metabolism, immunity-related traits[41,42], host genotypes, plant compartments (root, stem, or leaf tissues), and developmental stages, which are all host-specific determinants of plant-associated endophytic communities[30,43], we also hypothesize that the microbial community response may differ for distinct resistant konjac species and plant compartments. Finally, on the basis of the virulence mechanism of bacteriocins produced by *Pcc*, we believe that the response of the endophytic bacterial community to *Pcc* can be strengthened and that the fungal community may play an important role in resistance to *Pcc* infection. To test these hypotheses, we chose the main *Amorphophallus* species cultivated in China, *A. konjac* (susceptible), and a new germplasm resource, *Amorphophallus muelleri* (resistant), as experimental materials. We employed amplicon (bacterial and fungal) and metagenomic sequencing techniques to explore the differences in microbial community composition and functional profiles across different plant compartments (roots, petioles, and leaves) of susceptible and resistant konjac at different stages of *Pcc* infection. Additionally, we utilized traditional isolation-cultivation methods to investigate key populations influencing the interaction between *Pcc* and konjac. Our study results contribute to a deeper understanding of the assembly and functional adaptability of plant endophytic microbiomes under necrotic bacterial pathogen stress.

Results

Phenotypic differences between susceptible and resistant konjac under *Pcc* stress

Figure 1 shows the phenotypic differences between the susceptible species *A. konjac* and resistant species *A. muelleri* under *Pcc* stress. We found that 48 h after *Pcc* inoculation, *A. konjac* plants began to show obvious disease symptoms. Specifically, a thick liquid flowed out from the inoculation point, and the internal tissue of the petiole began to show water-soaked rot (Fig. 1c, d); at 96 h after *Pcc* inoculation, the internal tissue of the *A. konjac* petiole had rotted, turned black across a large area and become watery, leading to lodging symptoms in the whole plant (Fig. 1e). In contrast, the resistant species *A. muelleri* did not show any obvious symptoms at the inoculation site 48 h after *Pcc* inoculation, and only slight browning of the internal tissue of the petiole was observed (Fig. 1f, g); at 96 h after *Pcc* inoculation, the tissue near the inoculation site on the petiole presented brown lesions, but no signs of petiole tissue rot or lodging were observed (Fig. 1h). In previous studies, through combined analysis of the transcriptome, metabolome and microbiome (amplicon sequencing) of petiole tissue samples of two types of konjac, we found that, during the process of responding to *Pcc* infection, susceptible and resistant konjac species presented similar resistance responses at the transcriptional and metabolic levels, but there were significant differences in the regulation of the endogenous microbial community[44]. The resistant species *A. muelleri* tends to recruit more beneficial endophytic fungal taxa to resist *Pcc* infection. However, the previous study focused mainly on the petiole tissues of konjac as experimental materials. Konjac soft rot is a systemic disease caused by *Pcc*, which can infect all parts of konjac plants (leaves, petioles, roots, and tubers). It is largely unknown whether other plant tissues (such as roots and leaves) can use similar strategies to attract beneficial microorganisms to protect the host under pathogen infection. Therefore, this study focused on the in-depth examination of the community composition and functional adaptability of endogenous microorganisms in different plant compartments of the two types of konjac at different *Pcc* infection stages.

Factors affecting the assembly of the konjac microbiome

First, we carried out amplicon sequencing on 90 samples from different plant compartments of the two konjac species. To study the factors affecting the compositions of the endophytic microbial communities in konjac, we evaluated the relative contributions of various factors to the compositions of the endophytic microbial communities in konjac from the following perspectives: species (with different resistance levels), plant compartments and *Pcc* infection status. NMDS ordination and PERMANOVA revealed that the plant compartment had the greatest impact on the endophytic bacterial communities ($R^2 = 0.35$, $P < 0.001$), followed by *Pcc* infection ($R^2 = 0.12$, $P < 0.001$) and then the species ($R^2 = 0.04$, $P < 0.013$). In the fungal community, the plant compartment had the greatest impact ($R^2 = 0.29$, $P < 0.001$), followed by the species ($R^2 = 0.05$, $P < 0.001$) and *Pcc* infection ($R^2 = 0.01$, $P < 0.327$) (Fig. 2b; Supplementary Table 1). We further evaluated the effects of species and *Pcc* infection on the bacterial and fungal communities in different compartments. The results revealed that *Pcc* explained a greater proportion of the variation in the bacterial communities than in the fungal communities in the konjac leaf, petiole and root tissues. Furthermore, *Pcc* had the greatest effect on the bacterial community in the petiole, followed by the leaf and root. In contrast, the species explained a greater proportion of the variation in the fungal community than did *Pcc* infection (Supplementary Table 2).

A Venn diagram showing the effects of species, plant compartment and *Pcc* infection on the bacterial and fungal community compositions was prepared (Supplementary Fig. 1a, b). A total of 2349 bacterial and 2354 fungal OTUs were recovered from the samples from different compartments of the two species of *Amorphophallus*. Among them, 303 (bacterial) and 190 (fungal) OTUs were shared across different plant compartments. In comparison, *A. konjac* and *A. muelleri* shared 1414 (60.20%) bacterial and 917 (38.95%) fungal OTUs; there were 920 fungal OTUs unique to *A. konjac* (39.08%) and 517 fungal OTUs unique to *A. muelleri* (21.96%). However, there were no significant differences in the number of bacterial OTUs unique to the two species. The healthy (CK) and *Pcc*-infected groups shared 1327 (56.49%) bacterial and 1028 (43.67%) fungal OTUs. The number of fungal OTUs unique to the CK group was 808 (34.32%), and the number of fungal OTUs unique to the *Pcc* group was 518 (22.01%). These results indicated that under different grouping conditions (species, plant compartment and *Pcc* infection), the number of fungal OTUs specifically enriched in konjac tissues was greater than that enriched in bacteria.

Next, we evaluated the changes in the alpha diversity indices of the endophytic microbial communities in different compartments of the two konjac species in the different treatment groups (Fig. 2c, d). We found that inoculation with sterile water or *Pcc* could alter the diversity of bacterial and fungal communities in the leaf, petiole, and root tissues of both konjac species. After inoculation with sterile water, the Shannon index of bacterial communities in *A. konjac* petiole and root tissues showed significant reduction compared to the uninoculated control (H0) ($P < 0.05$) (Fig. 2c). Conversely, the Shannon index of fungal communities in *A. konjac* leaf tissues and the Chao1 index of fungal communities in *A. muelleri* petiole tissues demonstrated significant increases relative to the control ($P < 0.05$) (Fig. 2d). *Pcc* inoculation resulted in decreased Shannon and Chao1 indices for endophytic bacterial communities in petiole and root tissues of both *A. konjac* and *A. muelleri* when compared to both the uninoculated control and sterile water treatment. The Chao1 index of the endophytic bacterial community in *A. konjac* leaf tissues was significantly lower than that of the uninoculated control at 48 h after *Pcc* inoculation ($P < 0.05$). However, for *A. muelleri* leaf tissues, both the Shannon and Chao1 indices of the endophytic bacterial community tended to increase after *Pcc* inoculation compared with those of the uninoculated control. In particular, at 48 h after *Pcc* inoculation, these values were significantly greater than those of the uninoculated control ($P < 0.05$) (Fig. 2c). Notably, *Pcc* inoculation induced increasing trends in Shannon indices for endophytic fungal communities across all *A. konjac* tissues (leaf, petiole, and root) relative to the uninoculated control. These values reached statistical significance at 96 h after *Pcc* inoculation ($P < 0.05$) (Fig. 2d).

Composition of the konjac endophytic bacterial communities under *Pcc* stress

At the phylum level, the endophytic bacterial communities in konjac tissues subjected to different treatments were mainly composed of Proteobacteria (84.43 ± 14.53%) and Actinobacteria (8.61 ± 7.89%). The average relative abundance heatmaps of the top 30 bacterial genera in the groupwise

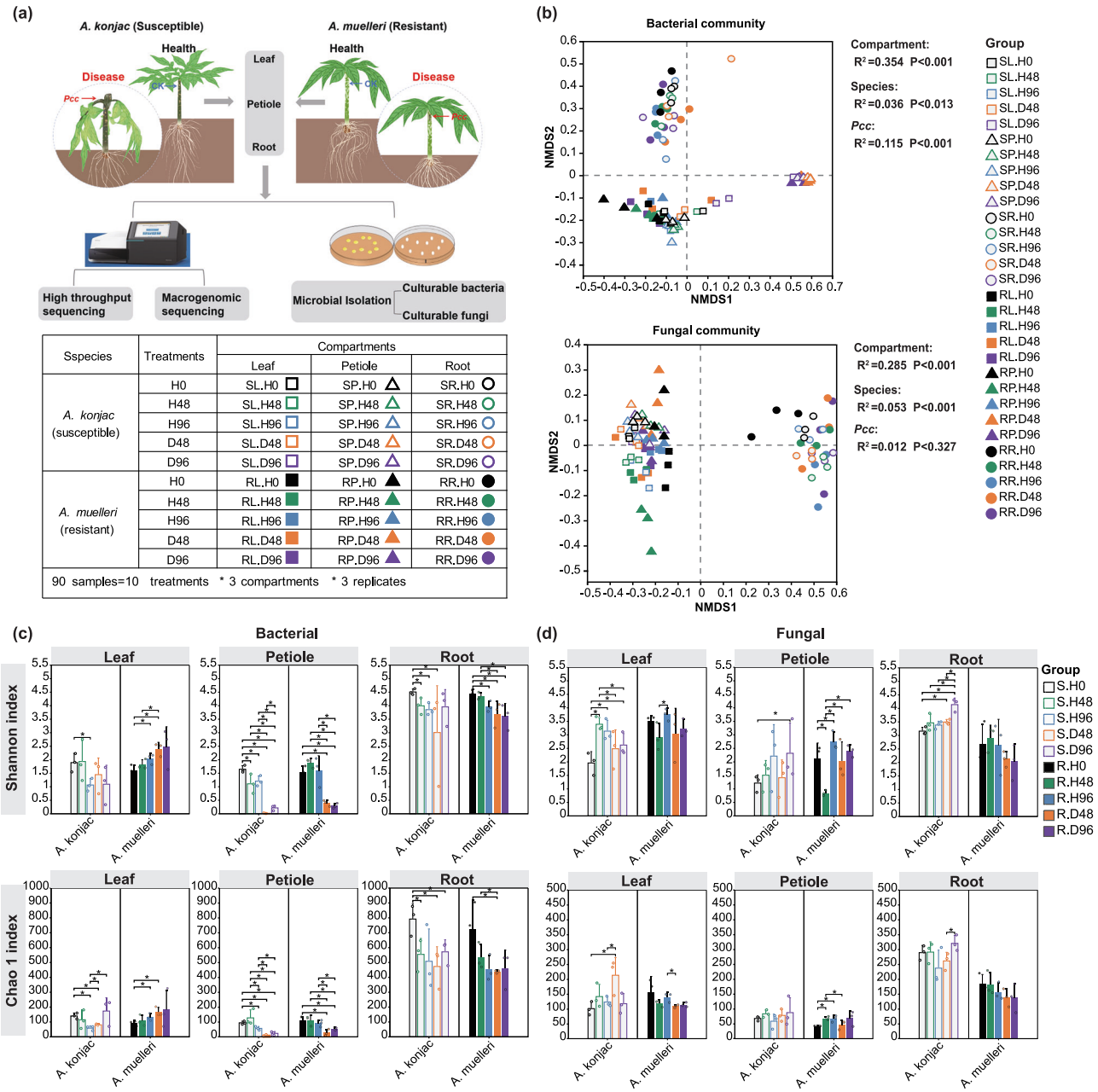

Fig. 2 | Factors affecting the composition of endophytic bacterial and fungal communities of konjac and the alpha diversity of the bacterial and fungal communities. a Experimental design of this study and information about the collected samples (Statement). **b** Nonmetric multidimensional (NMDS) ordinations of Bray–Curtis dissimilarity matrices with permutational analysis of variance (PERMANOVA), showing significant associations of the bacterial and fungal community compositions with, in order of importance, the compartment ($R^2 = 0.354$ for bacteria and $R^2 = 0.285$ for fungi), species ($R^2 = 0.036$ and 0.053), and *Pcc* infection ($R^2 = 0.115$ and 0.012), $n = 90$. **c**, **d** Shannon and Chao1 diversity indices of the bacterial and fungal communities in the different treatment groups, $n = 3$ biologically independent samples/group, error bars represent mean ± SD (Statement: the konjac illustrations in Fig. 2a are original artwork generated in Photoshop 2020, while sequencing equipment and petri dish images were obtained from Bing. The Shannon and Chao 1 indices of bacterial and fungal communities for samples SP.H0, SP.D48, SP.D96, RP.H0, RP.D48, and RP.D96 were also used in our previous work[44]).

comparison under different treatments are shown in Supplementary Fig. 2. The leaf tissues of the different treatment groups were divided into three main branches (Supplementary Fig. 2a). All treatment groups of *A. muelleri* were located in one large clade, where RL.D48 and RL.D96 were located on separate branches. In addition, SL.D96 was located in a separate clade that was significantly separated from the remaining four groups (SL.H0, SL.H48, SL.H96 and SL.D48). We observed that the relative abundance of *Sphingomonas* in the SL.D48 and SL.D96 groups was lower than that in the SL.H0, SL.H48, and SL.H96 groups ($P = 0.008$), and the relative abundance of *Aureimonas* in the RL.D48 and RL.D96 groups increased significantly compared with that in the RL.H0 group ($P = 0.003$) (Supplementary Fig. 2b).

In the petiole tissue, the samples of *A. konjac* and *A. muelleri* infected by *Pcc* (SP.D48, SP.D96, RP.D48, RP.D96) were located in the same clade, indicating that the microbial community compositions of the four treatment groups were more similar to each other yet significantly different from those of the uninoculated control and the samples inoculated with sterile water (Supplementary Fig. 2c). After inoculation with *Pcc*, the relative abundance of *Pectobacterium* in the petiole tissues of the two konjac species increased significantly, and this genus became dominant ($P = 0.004$).

Compared with those in the uninoculated control or the samples inoculated with sterile water, the relative abundances of many bacterial genera, such as *Sphingomonas*, *Pseudomonas*, *Rhodococcus*, and *Microbacterium*, tended to decrease after inoculation (Supplementary Fig. 2d).

In root tissues, we also observed that healthy and infected samples of the two konjac species clustered on distinct branches, indicating that there were large differences in the bacterial community compositions between the infected and healthy samples (Supplementary Fig. 2e). With respect to the relative abundance of species, we noted the relative abundance of *Flavobacterium* in the SR.D48, SR.D96, and RR.D96 groups showed an increasing trend compared with that in the uninoculated control. In particular, the relative abundance in SR.D48 was significantly greater than that in SR.H0 ($P < 0.05$). The relative abundance of *Methylobacillus* in the RR.D48 and RR.D96 groups increased significantly compared with that in the RR.H0, RR.H48, and RR.H96 groups. Meanwhile, regardless of *Pcc* infection, the relative abundance of *Methylobacillus* in the root tissues of *A. muelleri* was consistently greater than that in the root tissues of *A. konjac* (Supplementary Fig. 2f).

Composition of the konjac endophytic fungal communities under *Pcc* stress

The endophytic fungal communities in the leaf tissues of konjac are composed mainly of Tremellomycetes, Dothideomycetes, Cystobasidiomycetes, Sordariomycetes, and Agaricomycetes. The total average relative abundance of these five classes in the sequences of each sample was 84.49 ± 10.66% (Fig. 3a). We found that, compared with those in the SL.H0 group, the relative abundances of the classes Dothideomycetes and Sordariomycetes in the SL.H48 and SL.H96 groups increased significantly ($P < 0.05$). The relative abundances of the classes Dothideomycetes and Sordariomycetes in the SL.D48 and SL.D96 groups tended to increase compared with those in the SL.H0 group but were lower than those in the SL.H48 and SL.H96 groups ($P > 0.05$). We observed an increase in the relative abundance of Dothideomycetes and a decrease in the relative abundance of Sordariomycetes in the RL.H48, RL.H96, RL.D48, and RL.D96 groups compared with the RL.H0 group. We also found that the relative abundances of Dothideomycetes and Sordariomycetes were greater in the RL.D48 group than in the RL.H48 group, while they were lower in the RL.D96 group than in the RL.H96 group ($P > 0.05$) (Fig. 3b).

In petiole tissues, the endophytic fungal communities were composed mainly of Tremellomycetes, Cystobasidiomycetes, Dothideomycetes, Sordariomycetes, and Eurotiomycetes. The total average relative abundance of these five classes in the sequences of each sample was 93.68 ± 4.64% (Fig. 3c). We observed that the relative abundances of Dothideomycetes and Sordariomycetes in the SP.H96 and SP.D96 groups increased significantly compared with those in the SP.H0 group ($P < 0.05$). Similarly, the relative abundance of Dothideomycetes in the RP.H96 and RP.D96 groups was significantly greater than that in the RP.H0 group ($P < 0.05$). However, the relative abundance of Dothideomycetes in the SP.D96 and RP.D96 groups was lower than that in the SP.H96 and RP.H96 groups, respectively ($P > 0.05$). In addition, we found that the relative abundances of Dothideomycetes and Sordariomycetes in the SP.D48 and RP.D48 groups tended to increase compared with those in the SP.H0 and RP.H0 groups, respectively, but the differences were not significant (Fig. 3d).

In root tissues, Agaricomycetes, Glomeromycetes, Sordariomycetes, Dothideomycetes, and Eurotiomycetes were the top 5 fungal classes in terms of relative abundance. The total average relative abundance of these 5 classes in the sequences of each sample was 87.91 ± 8.08% (Fig. 3e). After inoculation with sterile water and *Pcc*, the relative abundances of the classes Agaricomycetes and Dothideomycetes in *A. konjac* tended to decrease compared with those in the uninoculated control. In particular, the relative abundance of Agaricomycetes in the SR.D96 group was significantly lower than that in the SR.H0 and SR.D48 groups ($P < 0.05$). In the root tissues of *A. muelleri*, the relative abundances of the classes Sordariomycetes, Dothideomycetes, and Eurotiomycetes all tended to decrease after inoculation with sterile water and *Pcc* compared with those in the uninoculated control, but the differences were not significant (Fig. 3f).

Cultivation and antagonistic effect evaluation of endophytic bacteria and fungi in konjac

To investigate the antibacterial effect of endophytic microorganisms in *A. konjac* and *A. muelleri*, a total of 82 bacterial isolates and 152 fungal isolates were obtained from different tissue samples (Fig. 4). We subsequently performed a *Pcc* antagonism assay to screen bacteria and fungi with the potential to inhibit the growth of *Pcc*. We observed that 46 fungal strains strongly inhibited the growth of *Pcc*, of which 18 strains were derived from *A. konjac* tissue samples, and 28 strains were derived from *A. muelleri* tissue samples (Fig. 4a, b; Supplementary Table 3). However, none of the 82 bacterial strains we isolated had inhibitory effects on the growth of *Pcc* (Fig. 4c). Moreover, we observed that only 5 out of the 18 strains from *A. konjac* tissue samples were derived from healthy, uninfected tissue samples, whereas 6 and 7 strains were derived from tissue samples that had been infected for 48 h and 96 h, respectively. Similarly, only 5 out of the 28 strains from *A. muelleri* tissue samples were derived from healthy, uninfected tissue samples, whereas 4 and 19 strains were derived from infected tissue samples at 48 h and 96 h, respectively. The isolation rates of antagonistic strains from healthy tissue samples of *A. konjac* and *A. muelleri* were 27.78% and 17.86%, respectively, while the isolation rates of antagonistic strains from *A. konjac* and *A. muelleri* samples infected with *Pcc* were 72.22% and 82.14%, respectively.

We preliminarily identified the isolated *Pcc* antagonistic fungal strains by ITS region analysis. The results revealed that the 46 fungal strains belonged to three classes: Dothideomycetes, Sordariomycetes and Eurotiomycetes. At the genus level, these isolates were classified into 14 fungal genera, including *Cladosporium* spp., *Pseudopithomyces* spp., *Stagonosporopsis* spp., *Didymella* spp., *Setophoma* spp., *Paraconiothyrium* spp., *Phaeosphaeria* spp., *Alternaria* spp., *Clonostachys* spp., *Sarocladium* spp., *Aspergillus* spp., *Penicillium* spp., and *Talaromyces* spp. In this study, the *Trichoderma* spp. strains had the highest isolation rates, accounting for 30.43% of the total antagonistic fungal strains, followed by *Cladosporium* spp. strains, accounting for 19.57% of the total number of antagonistic fungal strains.

We further performed phylogenetic analysis on the basis of the amplicon sequencing results. The results revealed that the strains of the genera *Cladosporium*, *Penicillium*, *Aspergillus*, *Alternaria*, *Sarocladium*, *Trichoderma*, *Stagonosporopsis*, and *Setophoma*, which were identified via amplicon sequencing, were all successfully isolated (Fig. 4d; Supplementary Figs. 3 and 4). Coincidentally, the results of amplicon sequencing revealed that the relative abundance of *Cladosporium* in leaf tissue ranked among the top 3 (Fig. 4d). We also found that the isolation rate of *Cladosporium* strains was the highest in leaf tissue. In petiole tissue, the isolation rate of *Trichoderma* was the highest. Moreover, the results of amplicon sequencing revealed that the relative abundance of *Trichoderma* was highest in the SP.D48 sample, followed by the RP.D96 and RP.H0 samples (Supplementary Fig. 3). In this study, the *Trichoderma* strains isolated from petiole tissue mainly originated from the above three samples. The above results indicate that our isolation results are highly consistent with the amplicon sequencing results, especially for the leaf and petiole tissues.

Cooccurrence networks of konjac microbial communities under *Pcc* stress

To investigate the impact of *Pcc* on the co-occurrence patterns of konjac microbial communities, we separately analyzed the bacterial–bacterial and fungal–fungal intradomain networks and the bacterial–fungal interdomain network of three compartments in susceptible and resistant konjac plants at different infection stages (Figs. 5 and 6; Supplementary Fig. 5). The results of the intradomain network analysis revealed that, compared with those of the uninoculated plants, under *Pcc* stress, the numbers of nodes and edges in the bacterial intradomain network within the root, petiole and leaf tissues of *A. konjac* tended to decrease, whereas the numbers of nodes and edges in the

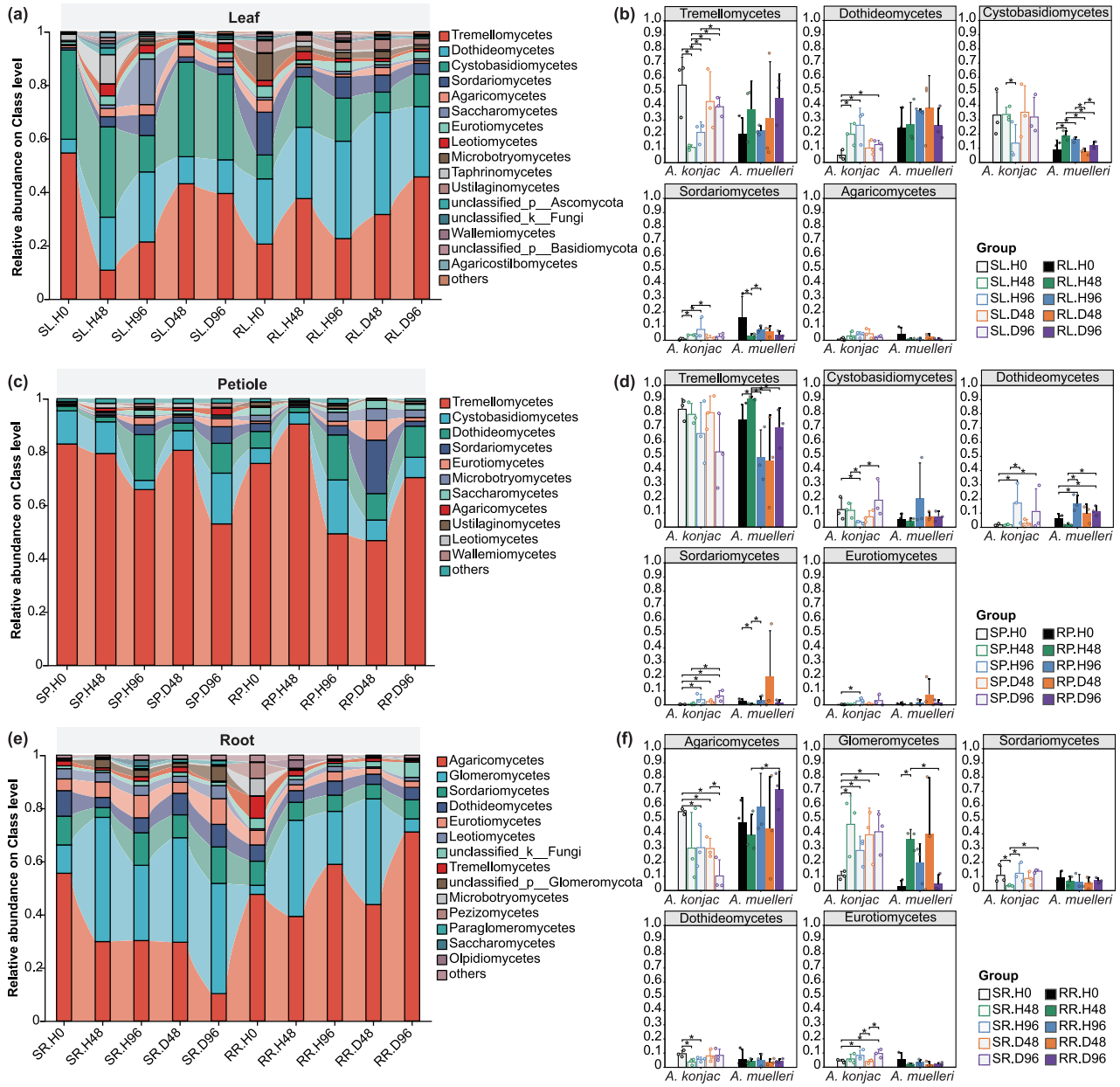

Fig. 3 | Fungal class composition and relative abundance in konjac tissues under different treatments. a, **c**, **e** Composition in leaf, petiole, and root tissues. Classes with less than 1% of the total reads were grouped into "others". **b**, **d**, **f** The bar plots show the differences in the relative abundances of the top 5 fungal classes among the different treatment groups, $n = 3$ biologically independent samples/group, error bars represent mean ± SD.

fungal intradomain network tended to increase (Supplementary Tables 4–6). The petiole tissue of the resistant species *A. muelleri* showed a similar trend, with a decrease in the number of nodes and edges in the bacterial intradomain network but an increase in the number of nodes and edges in the fungal intradomain network (Supplementary Table 4). In contrast, in the leaf tissue, the number of nodes and edges in the bacterial intradomain network increased, whereas the number of nodes and edges in the fungal intradomain network decreased (Supplementary Table 5). In the root tissue, the number of nodes and edges in both the bacterial and fungal intradomain networks decreased (Supplementary Table 6). The intradomain correlations in the healthy and diseased networks of the two konjac species were mainly positive correlations. Interestingly, the complexity of the fungal intradomain network appeared to be associated with the severity of *Pcc* infection in the host plants. Compared with those of the resistant *A. muelleri* plants, the root, petiole, and leaf tissues of the susceptible *A. konjac* plants after 48 h of infection presented more nodes and edges in the fungal intradomain network, as well as a greater average degree. Similarly, in resistant *A. muelleri* plants, the number of nodes and edges in the fungal intradomain network gradually increased in the infected petiole and leaf tissues from 48 to 96 h post infection. Consistent with the symptoms observed, the disease severity in susceptible *A. konjac* plants was greater than that in resistant *A. muelleri* plants at 48 h of infection.

The analysis of interdomain ecological networks between bacteria and fungi revealed that *Pcc* stress disrupted the stability of the network. At 48 and 96 h of *Pcc* infection, both the number of nodes and edges and the average degree in the petiole tissue networks of the two species of konjac were lower than those in the healthy networks. Furthermore, the interdomain correlations were predominantly negative, and the proportion of negative edges was greater than that in the healthy networks (Fig. 5; Supplementary Table 4). In the leaf tissue, the numbers of nodes and edges in the interdomain network of the two species of konjac at 48 h and 96 h of *Pcc* infection were greater than those in the healthy networks, but again, the interdomain

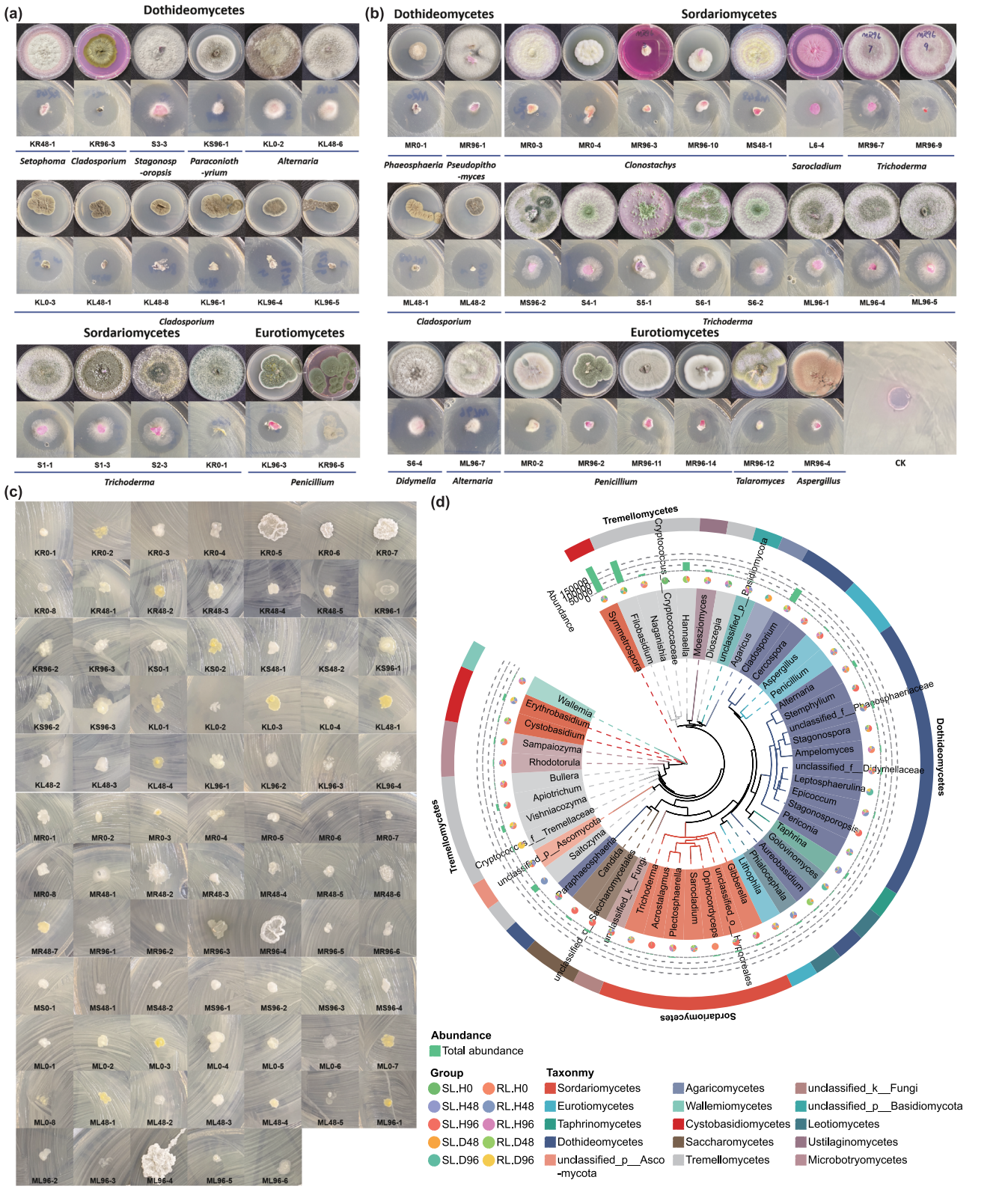

Fig. 4 | Culture and phylogenetic analysis of endophytic bacteria and fungi from *A. konjac* (susceptible) and *A. muelleri* (resistant) plants. a Eighteen fungal strains isolated from *A. konjac* tissue, which included strains from three classes, Dothideomycetes (12), Sordariomycetes (4) and Eurotiomycetes (2), inhibited Pcc growth. **b** Twenty-eight fungal strains, including 6, 16, and 6 strains from Dothidomycetes, Sortariomycetes, and Eurotioomycetes respectively, isolated from *A. muelleri* tissue inhibited *Pcc*. The first row shows the colony morphology of each fungal strain cultured on PDA/rose bengal agar for 7 days, and the second row shows the antagonistic activity of each strain against *Pcc*. The fungal species names and inhibition spectra (cm) of different fungal strains are provided in Supplementary Table 3. **c** Eighty-two bacterial strains isolated from *A. konjac* and *A. muelleri* tissues did not have any antagonistic effects on *Pcc*. **d** Phylogenetic trees showing the diversities of leaf-associated fungal communities at the genus level on the basis of amplicon sequencing results.

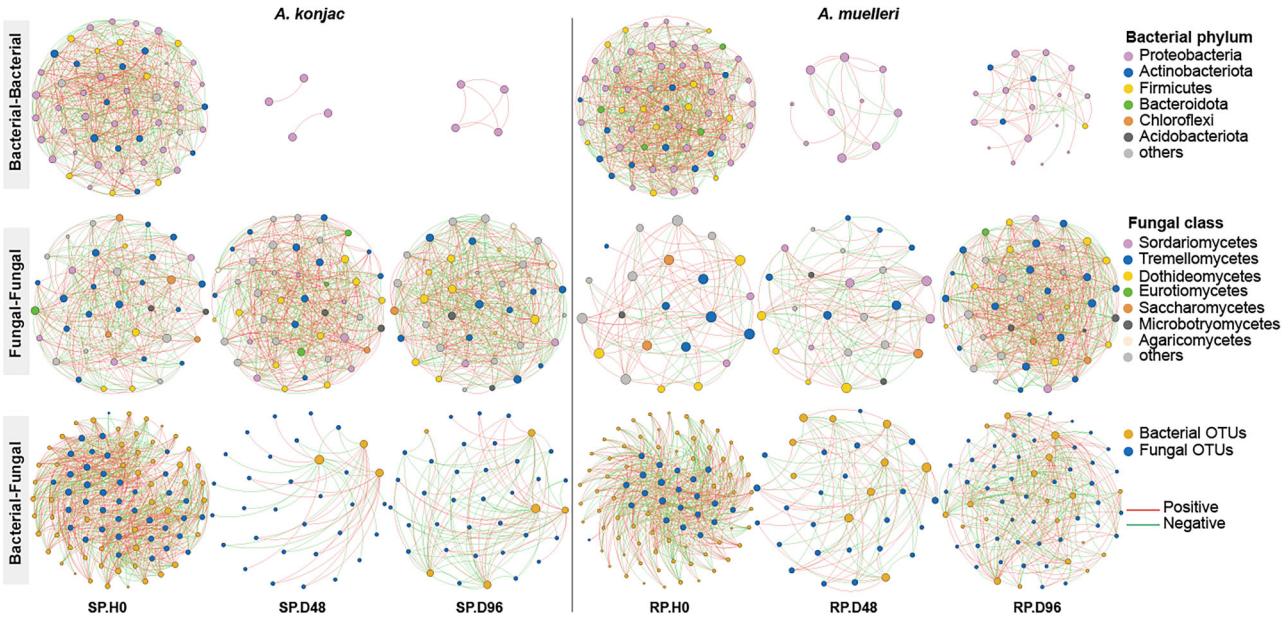

Fig. 5 | Cooccurrence network of microbial communities in the petiole tissues of konjac at different stages of *Pcc* infection. Intradomain network analysis showing a greater number of nodes and edges in fungal networks than in bacterial networks at 48 h and 96 h post infection. The nodes are colored according to bacterial phylum and fungal class. The edge color represents positive (red) and negative (green) correlations. Interdomain network analysis between bacteria and fungi showed a lower number of nodes and edges in diseased networks than in healthy networks, with a greater proportion of negative edges in diseased networks than in healthy networks.

correlations were mainly negative (Fig. 6; Supplementary Table 5). In root tissues, the number of nodes and edges in the resistant species *A. muelleri* were lower after 48 and 96 h of infection than those in the healthy network. On the other hand, in the susceptible species *A. konjac*, the number of nodes and edges was lower after 48 h of infection but greater after 96 h of infection than that in the healthy network (Supplementary Fig. 5; Supplementary Table 6).

Functional composition of konjac microbial communities under *Pcc* stress

We conducted metagenomic sequencing on root (underground) and petiole tissue (aboveground) samples from the uninoculated, *Pcc*-inoculated 48 h, and *Pcc*-inoculated 96 h groups to further explore the potential functional shifts in the microbial communities associated with konjac under *Pcc* infection. On the basis of the metagenomic sequencing results, 5679 bacterial and 392 fungal species were identified. We observed that the phylum Pseudomonadota was overwhelmingly dominant in the petiole tissues of *A. konjac*, accounting for an overall average relative abundance of 99.93 ± 0.02% in each sample (Fig. 7a). After inoculation with *Pcc*, the relative abundance of Pseudomonadota in the petiole tissues of *A. muelleri* increased by 12.17 ~ 12.24% compared with that in the uninoculated control ($P = 0.008$) (Supplementary Fig. 6a). Additionally, after *Pcc* inoculation, the relative abundance of Dothideomycetes in the petiole tissues of both konjac species tended to increase compared with that in the uninoculated control ($P = 0.175$) (Fig. 7a, Supplementary Fig. 7a). In the root tissues, the relative abundances of the phylum Pseudomonadota ($P = 0.012$) and the class Glomeromycetes ($P = 0.007$) increased in both konjac species after *Pcc* inoculation (Supplementary Figs. 6b, 7b and 8a), whereas the relative abundances of the classes Agaricomycetes ($P = 0.007$) and Dothideomycetes ($P = 0.023$) decreased after *Pcc* inoculation (Supplementary Fig. 7b). These observations were consistent with the amplicon sequencing data.

Metagenomic analysis revealed that the NMDS ordination of the KO, COG, and CAZy functional compositions of the petiole tissue microbiome of uninoculated *A. muelleri* (RP. H0) was significantly distinct from those of the other five treatments (Fig. 7b, Supplementary Fig. 9a). Additionally, the NMDS ordination of CAZy functions in RP.D48 and RP.D96 also showed separation from the remaining four treatments (Supplementary Fig. 9a). However, no significant separation was observed in the NMDS ordination of KO, COG, and CAZy functions among the three treatment groups SP.H0, SP.D48, and SP.D96. In petiole tissue, *A. muelleri* presented greater functional diversity of microbial communities after infection, with the Shannon indices of the KO and COG functions in RP.D48 and RP.D96 samples significantly increasing compared with those in RP.H0 ($P < 0.05$). In contrast, the functional diversity of the microbial communities in *A. konjac* tended to decrease after infection; in particular, the Chao index of KO functions in the SP.D48 and SP.D96 samples was significantly lower than that in the SP.H0 samples ($P < 0.05$) (Fig. 7c). The KO, COG, and CAZy functional compositions of the microbiomes in the root tissues of the two konjac species were separated along the NMDS2 axis, suggesting functional differences in the root tissue microbiomes between the two species. Additionally, the NMDS ordination of the KO, COG, and CAZy functions in the root tissue of *A. muelleri* (RR.H0, RR.D48, and RR.D96) also showed significant separation, with the three treatment groups clustering into distinct groups, further indicating functional differences in the microbiomes among the different treatment groups of *A. muelleri* (Supplementary Figs. 8b and 9b). The Chao and Shannon indices of the KO and COG functions in SR.D96 were significantly increased compared to those in SR.H0 and SR.D48 ($P < 0.05$). In contrast, the Shannon index of CAZy functions in RR.D96 was significantly lower than that in RR.H0 ($P < 0.05$) (Supplementary Fig. 8c).

To determine how *Pcc* affects the functional characteristics of the microbiome, we performed differential abundance analysis. The bar chart illustrates the significant differences in the relative abundances of the top 10 COG and CAZy functions among the different groups. In petiole tissue, the relative abundances of microbial functional genes associated with transcription (COG_K), inorganic ion transport and metabolism (COG_P), cell wall/membrane/envelope biogenesis (COG_M), translation, ribosomal structure, and biogenesis (COG_J), and coenzyme transport and metabolism (COG_H) were significantly increased in RP.D48 and RP.D96 samples compared with RP.H0 samples ($P < 0.05$), whereas the relative abundances of genes related to amino acid transport and metabolism (COG_E), carbohydrate transport and metabolism (COG_G), signal transduction mechanisms (COG_T), and energy production and conversion (COG_C) were significantly decreased compared to those in RP.H0 samples ($P < 0.05$).

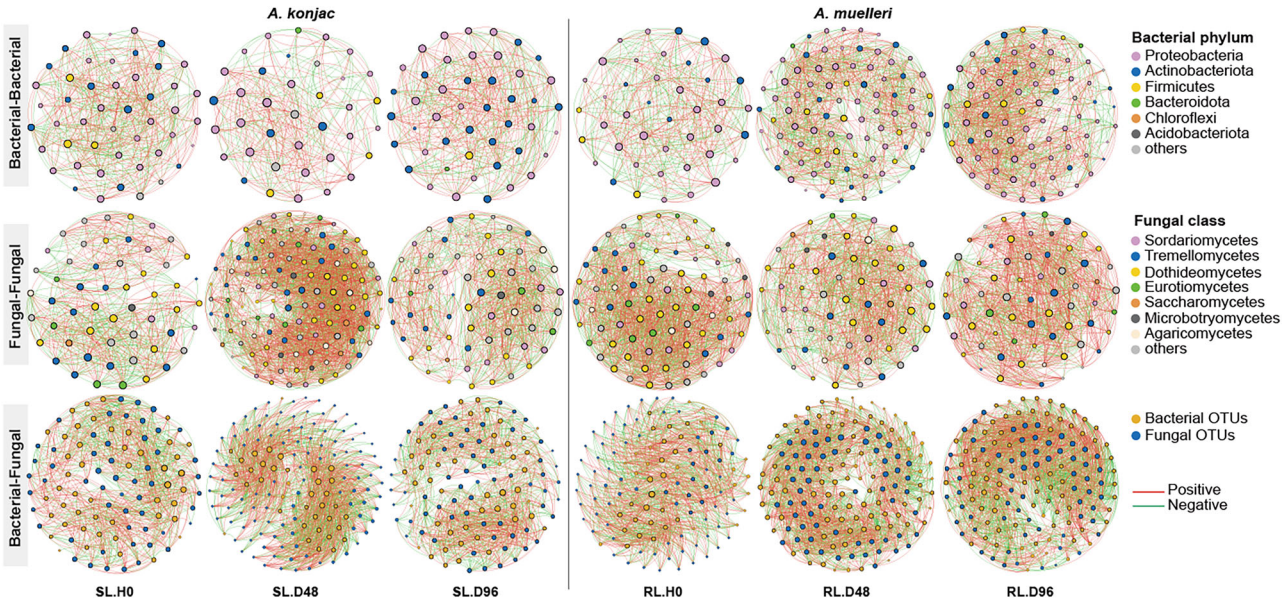

Fig. 6 | Cooccurrence network of microbial communities in the leaf tissues of konjac at different stages of *Pcc* infection. Intradomain network analysis of *A. konjac* showed a lower number of nodes and edges in the bacterial disease network but a greater number of nodes and edges in the fungal disease network than in the healthy network. Intradomain network analysis of *A. muelleri* showed a greater number of nodes and edges in the bacterial disease network and a lower number of nodes and edges in the fungal disease network than in the healthy network. Interdomain network analysis between bacteria and fungi showed that the diseased network presented greater numbers of nodes and edges and a greater proportion of negative edges than the healthy network.

In *A. konjac*, the relative abundance of genes associated with carbohydrate transport and metabolism (COG_G) was significantly greater in the SP.D48 and SP.D96 samples than in the SP.H0 samples ($P < 0.05$), whereas the relative abundance of genes related to signal transduction mechanisms (COG_T) was significantly lower than that in the SP.H0 samples ($P < 0.05$) (Fig. 7d, Supplementary Table 7). With respect to CAZy functions, the relative abundance of many glycoside hydrolases and glycosyl transferases in the petiole tissue of *A. muelleri* tended to increase after infection. For example, the relative abundances of the CE1 family, GT41 family, GH1 family, GT9 family, GH24 family, GH28 family, and GH109 family in RP.D48 and RP.D96 samples increased by 44.90–6860.00% compared to those in RP.H0 samples ($P < 0.05$). In *A. konjac*, we only observed that the relative abundances of the GH1 family and GH28 family in the SP.D48 and SP.D96 samples increased by 17.57–24.27% compared with those in the SP.H0 samples ($P < 0.05$). Additionally, we found that the CE1 family and GT41 family exhibited opposite trends in the two konjac species. The relative abundances of the CE1 family and GT41 family in the RP.D48 and RP.D96 samples increased by 69.85–337.45% compared with those in the RP.H0 samples ($P < 0.05$), whereas those in the SP.D48 and SP.D96 samples decreased by 2.56–9.13% compared with those in the SP.H0 samples ($P > 0.05$) (Fig. 7e, Supplementary Table 8).

In the root tissue, the relative abundances of microbial functional genes associated with signal transduction mechanisms (COG_T) and cell wall/membrane/envelope biogenesis (COG_M) in the infected *A. muelleri* RR.D48 and RR.D96 samples tended to increase compared to those in RR.H0 ($P < 0.05$); however, the relative abundances of genes related to amino acid transport and metabolism (COG_E), carbohydrate transport and metabolism (COG_G), and lipid transport and metabolism (COG_I) tended to decrease compared with those in the RR.H0 ($P < 0.05$). In *A. konjac*, after infection, we observed an increase in the relative abundances of genes associated with amino acid transport and metabolism (COG_E), signal transduction mechanisms (COG_T), inorganic ion transport and metabolism (COG_P), and lipid transport and metabolism (COG_I) in the SR.D48 and SR.D96 samples, as well as a decrease in the relative abundances of genes related to carbohydrate transport and metabolism (COG_G) and transcription (COG_K) (Supplementary Fig. 8d; Supplementary Table 9). Additionally, the relative abundances of the GT41 family significantly increased in both *A. konjac* and *A. muelleri* after infection compared with those in the uninoculated control ($P < 0.05$), whereas the relative abundances of the GH2 family and AA3_1 family decreased compared with those in the control (Supplementary Fig. 8e; Supplementary Table 10).

Finally, we analyzed the changes in the relative abundances of several methyl-accepting chemotaxis protein (MCP)-related genes. We found that the relative abundance of mcp (K03406) in the RP.H0 samples (84.16%) was significantly greater than that in the SP.H0 samples (62.83%). After infection, the relative abundances of mcp in RP.D48 and RP.D96 decreased compared with those in RP.H0 ($P < 0.05$), whereas those in SP.D48 and SP.D96 tended to increase compared with those in SP.H0. Additionally, we observed that the relative abundances of methyl-accepting chemotaxis protein II, aspartate sensor receptor (tar, K05875), and methyl-accepting chemotaxis protein III, ribose and galactose sensor receptor (trg, K05876), genes increased in the petiole tissues of both *A. konjac* and *A. muelleri* after infection ($P < 0.05$). In contrast, the relative abundances of functional genes downstream of MCPs, such as the two-component system, chemotaxis family, sensor kinase CheA (K03407) and purine-binding chemotaxis protein CheW (K03408), tended to decrease (Supplementary Table 11). With respect to the root tissue, the relative abundances of mcp in the SR.D96 samples, as well as the methyl-accepting chemotaxis protein I, serine sensor receptor (tsr, K05874), tar, and CheA in the SR.D48 samples, significantly increased compared to those in SR.H0. However, no significant differences were observed in the relative abundances of the MCP, CheA, and CheW genes among RR.H0, RR.D48, and RR.D96 (Supplementary Table 12).

Discussion

Pectobacterium spp. are considered among the ten most dangerous plant pathogenic bacteria[8]. These destructive bacterial pathogens persist in soil for long periods, making disease management almost impossible[45]. Regulation of the plant microbiota is increasingly being recognized as an environmentally sustainable method for protecting plants from diseases and promoting agricultural production. In recent years, a growing number of studies have emphasized that plant microbiome assembly and niche occupation significantly differ under various health and disease conditions[46–49]. In addition, some scholars have noted that disease may attenuate the plant

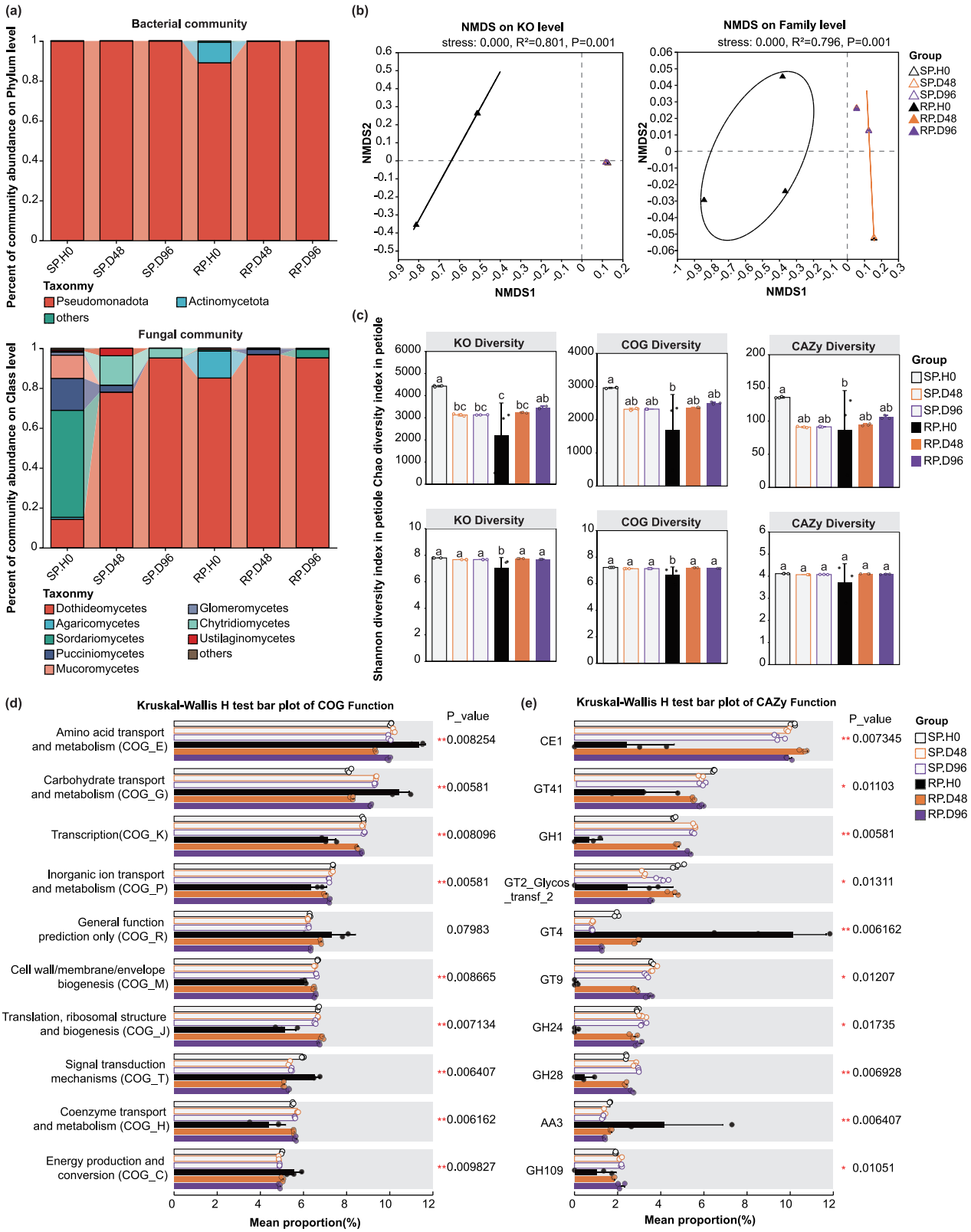

Fig. 7 | Microbiome functional diversity and differential abundance of functional genes/modules based on KO, COG, and CAZy functional profiles in the petiole tissues of susceptible and resistant konjac under *Pcc* stress. a Taxonomic composition of bacterial and fungal communities in petiole tissues of different treatment groups on the basis of metagenomic sequencing data, $n = 3$ biologically independent samples/group. **b** NMDS ordinations of functional genes on the basis of Bray–Curtis distance matrices of KO and CAZy (family-level) functional genes. **c** Shannon and Chao diversity indices of KO, COG, and CAZy functional genes in different treatment groups, $n = 3$ biologically independent samples/group. **d** Differential abundance analysis of COG functional modules between the different treatment groups, $n = 3$ biologically independent samples/group. **e** Differential abundance analysis of CAZy functional genes between the different treatment groups, $n = 3$ biologically independent samples/group. Error bars represent mean ± SD.

effects, thereby enhancing the differences in communities between diseased and healthy plants[11]. In this study, we found that under artificial inoculation with *Pcc*, the microbial community compositions of healthy and infected plants, both susceptible and resistant konjac, significantly differed. In particular, *Pcc* explained a greater proportion of the variation in the bacterial communities than that in the fungal communities in the leaf, petiole, and root tissues of the two species of *Amorphophallus*. These results suggested that, compared with those in the fungal communities, the variations in the endophytic bacterial communities of konjac were relatively large during infection by necrotic bacterial pathogens. This phenomenon could be closely related to the pathogenic mechanism of *Pcc*. *Pcc* often secretes bacteriocins to improve its competitiveness with related competing species[9,10]. In this study, we observed that after *Pcc* infection, the Shannon and Chao1 indices of endophytic bacterial communities in both the petiole and root tissues of susceptible and resistant konjac plants decreased compared with those in the uninoculated controls. Furthermore, in the petiole tissues, which were the most severely infected, *Pectobacterium* dominated overwhelmingly, while the relative abundances of most bacterial taxa, such as *Sphingomonas*, *Pseudomonas*, and *Bacillus*, in infected plants were drastically reduced compared with those in healthy plants.

In bacteria, MCPs are important membrane-bound receptors. When specific chemicals, such as sugars, amino acids, and organic acids, are detected, MCPs respond to a signaling pathway consisting of the CheABRWYZ proteins[50], eventually changing the rotation direction of the bacterial flagella and inducing a chemotaxis behavior of approach or retreat. Chemotaxis is an important process involving a variety of host–pathogen interactions that ultimately determine the outcome of infection[51,52]. In this study, we observed significant changes in MCPs and their downstream functional genes in the petiole tissues of both susceptible and resistant *Amorphophallus* species after *Pcc* infection. Many plant pathogens are predicted to encode more than 30 MCP receptors, and *Pectobacterium* spp. have been reported to encode 30–39 tropic receptors[53,54]. Moreover, MCPs have been identified in typical beneficial bacteria, such as *Pseudomonas* spp[55,56]. and *Bacillus subtilis*[57]. Our results supported the substantial changes in the relative abundance of MCP-producing bacteria (such as *Pectobacterium*, *Bacillus*, *Pseudomonas*, etc.) in the two konjac tissues under *Pcc* stress, suggesting that the enrichment of MCP genes in diseased plants could be related to the responses of these bacteria to the signaling molecules released by plants. This relationship could arise because chemotaxis usually occurs when bacterial cells move along chemical gradients to find a favorable environment or attempt to escape from an unfavorable environment. This phenomenon could be an important reason why the variations in bacterial communities in konjac tissues were greater than those in fungal communities after *Pcc* infection. Overall, our results suggest that infection by the necrotrophic bacterial pathogen *Pcc* induces significant changes in the endophytic bacterial communities of both susceptible and resistant *Amorphophallus* species, thereby enhancing the differences between the microbial communities of diseased and healthy plants.

In the plant-associated microbiota, some central microbes can affect community structure through strong biotic interactions with the host or other microbial species, rather than simply by affecting community structure through their high abundance[11]. Through these central microbes, host plants can selectively influence the structures of their associated microbiota by regulating the interactions between microbes and altering host adaptation[29,58]. This study revealed that in the petiole tissues of both *Amorphophallus* species at 48 h and 96 h postinfection, the number of nodes and edges in the bacterial intradomain networks was lower than that in the networks of healthy plants. In contrast, the number of nodes and edges in the fungal intradomain networks increased, and the average connectivity was also greater than that in networks of healthy plants. The increase in the number of nodes, edges and connections in the fungal intradomain network suggests the ecological importance of fungal taxa in response to *Pcc* stress. On the other hand, after *Pcc* infection, the proportion of negative correlations in the bacterial-fungal interdomain networks increased in the root, petiole, and leaf tissues of both *Amorphophallus* species. Cooperative and competitive interactions among microbial species can influence community stability, and the observed negative interactions represent ecological competition between bacteria and fungi[59]. The host could benefit from the microbial competition, resulting in improved resistance to external stress[60]. Interestingly, through the isolation of culturable microorganisms and antagonism assays, we further demonstrated that fungal taxa such as *Trichoderma*, *Cladosporium*, and *Penicillium* in the tissues of both *Amorphophallus* species strongly inhibited the growth of *Pcc*. Moreover, the isolation rates of these antagonistic fungal strains were greater in the infected tissue samples of both *Amorphophallus* species than in the healthy tissue samples. Among the antagonistic strains we isolated, species such as *Trichoderma*, *Talaromyces*, and *Penicillium* have been reported as plant probiotics that play important roles in regulating host performance, particularly in the suppression of plant pathogens[61–63]. Phylogenetic analysis revealed that the antagonistic strains we isolated belonged primarily to three classes: Dothideomycetes, Sordariomycetes, and Eurotiomycetes. On the basis of the amplicon and metagenomic sequencing results, we further revealed that the classes Dothideomycetes and Sordariomycetes, as core taxa, were present in the treated *Amorphophallus* plant samples and that the relative abundances of these core taxa exhibited dynamic changes across the different treatments. Our results further demonstrated that the changes in the core endophytic microbial community in *Amorphophallus* tissues differed after inoculation with sterile water and the *Pcc* suspension. These results suggest that under necrotrophic bacterial pathogen stress, endophytic fungal communities in *Amorphophallus* species may protect the host plant through ecological competition or by inhibiting pathogen growth. However, the emphasis on the functions of these communities through antagonist experiments alone remains limited. In the future, we could comprehensively analyze the relevant functions from multiple perspectives, such as field testing, strain genome sequencing, and metabolite detection.

The ecological functions of plants, including defense against pathogens, can be implemented through the synergy of the plant microbiota. The plant core microbiota consists of members of the microbial community that are persistent and ubiquitous in almost all the communities associated with a particular host[64,65]. The core microbiota contains key microbial taxa that carry genes with functions that are essential for host fitness[66]. Metagenomic analysis revealed that the KO, COG, and CAZy functional diversities in the petiole tissue microbiome of *A. konjac* decreased to varying degrees after *Pcc* infection compared with that in healthy plants, whereas the functional diversity in the resistant species *A. muelleri* tended to increase compared with that in healthy plants. Higher functional diversity of the microbiome promotes its participation in multiple ecosystem functions[36].

After *Pcc* infection, microbial functional genes associated with modules such as translation, ribosomal structure and biogenesis, cell wall/membrane/envelope biogenesis, inorganic ion transport and metabolism, and coenzyme transport and metabolism were enriched in the root and petiole tissues of *A. muelleri*. Pathogen infection typically induces changes in the internal microenvironment of the plant. Specifically, during *Pcc* infection, the secretion of large amounts of pectinases and bacteriocins disrupts the ion balance within plant cells[67]. The enrichment of microbial functional genes related to translation, ribosomal structure and biogenesis, and cell wall/membrane/envelope biogenesis in *A. muelleri* plants helps protect against the normal progression of intracellular physiological activities, thereby increasing the adaptability of endophytic microorganisms to environmental changes[68]. On the other hand, the enrichment of genes associated with inorganic ion transport and metabolism, as well as coenzyme transport and metabolism, helps maintain the ion balance of plant cells, regulate plant immune signaling, and induce plant defense responses[69]. In contrast, we did not observe significant changes in the aforementioned microbial functional genes in *A. konjac* plants. After infection, we only observed significant enrichment of microbial functional genes related to carbohydrate transport and metabolism, as well as a significant reduction in genes associated with signal transduction mechanisms, in the petiole tissues of *A. konjac*. Plant cell walls are essential elements for disease resistance that pathogens need to overcome to colonize the host. These walls are primarily composed of

carbohydrate-based polymers (cellulose, hemicelluloses, and pectins), which consist of distinct monosaccharide moieties linked by different types of bonds[70]. Some pathogens overcome these resistance barriers by breaking down cell wall polysaccharides through the coordinated action of cell wall-degrading/modifying enzymes (CWDEs)[71]. This is precisely the case with *Pcc*, which secretes a series of extracellular pectinases to degrade the plant cell wall, thereby facilitating infection and causing harm to the plant[9,10]. *Pcc* secretes a large number of enzymes to hydrolyze plant cell wall polysaccharides, leading to the release of carbohydrate molecules (glycans). These molecules are perceived by plant pattern recognition receptors, which in turn activate pattern-triggered immunity and disease resistance[72]. Therefore, the significant enrichment of microbial genes associated with carbohydrate transport and metabolism modules in the petiole tissues of *A. konjac* following infection is closely related to the extensive colonization of *Pcc* within the petiole tissues of *A. konjac*. Our amplicon sequencing results revealed that *Pcc* dominated the petiole tissues of *A. konjac* after infection, whereas in tissues with relatively lower *Pcc* contents (root tissues of *A. konjac*, as well as petiole and root tissues of *A. muelleri*), the relative abundance of carbohydrate transport and metabolism genes decreased compared with those in the uninoculated controls.

We also observed significant differences in CAZy-related functional genes between sensitive and resistant *Amorphophallus* species under *Pcc* stress. Notably, the relative abundance of the CE1 family in the petiole tissues of the two *Amorphophallus* species exhibited completely opposite trends after infection: it significantly increased in *A. muelleri* but decreased in *A. konjac*. Carbohydrate esterases, encompassing 16 recognized CEs, are a class of enzymes that remove ester groups from carbohydrates[72]. The CE1 family is one of the largest and most diverse CE families and includes acetylxylan esterases (EC 3.1.1.72), feruloyl esterases (EC 3.1.1.73), carboxylesterases (EC 3.1.1.1), S-formylglutathione hydrolases (EC 3.1.2.12), diacylglycerol O-acyltransferases (EC 2.3.1.20), and trehalose 6-O-mycolyltransferases (EC 2.3.1.122)[73]. Among these enzymes, acetylxylan esterases (AXEs, EC 3.1.1.72) catalyze the hydrolysis of acetyl groups in xylan, whereas feruloyl esterases (FAEs, EC 3.1.1.73) release ferulic acid and other hydroxycinnamic acids from xylan and pectin[74]. Ferulic acid, a key phenolic compound, can enhance plant disease resistance and cell wall defense capabilities through multiple mechanisms. For example, ferulic acid increases the mechanical strength and stability of the cell wall by forming cross-linked networks with hemicellulose (such as xylan) and lignin. Additionally, ferulic acid is one of the precursors for lignin biosynthesis, and an increase in the ferulic acid content can promote lignin deposition[73]. Coincidentally, in a previous study, we utilized LC/MS-MS to analyze changes in metabolites in the petiole tissues of two *Amorphophallus* species at different *Pcc* infection stages. We observed that the levels of several lignin precursors, such as ferulic acid, sinapic acid, and syringin, tended to increase in both species after infection. Moreover, at different infection stages (0 hpi, 48 hpi, and 96 hpi), the contents of these substances in the petiole tissues of the resistant species *A. muelleri* were consistently greater than those in the susceptible species *A. konjac*[44]. Therefore, we hypothesize that the significant enrichment of microbial functional genes in the CE1 family in this study was associated with the reinforcement of the plant cell wall in *A. muelleri* after infection. Consistent with the disease symptoms of the two *Amorphophallus* species, we did not observe ulceration in the petiole tissue of *A. muelleri* after *Pcc* infection, whereas *A. konjac* exhibited complete disintegration of the petiole tissue with water-stained rot (plant lodging) at 96 h post infection.

Finally, we noted that the response of the endophytic microbial communities in the root tissues of the two *Amorphophallus* species to *Pcc* was not as pronounced as that in the petiole tissues. This was likely the effect of our experimental method, as in this study, the pathogen *Pcc* was inoculated primarily into the petiole region. However, we also observed significant changes in the levels of microbial functional genes related to chemotaxis and signal transduction mechanisms, such as MCPs, cheA, and cheW, in the root tissues of both *Amorphophallus* species. Specifically, the relative abundance of chemotaxis-related genes, including mcp, tsr, tar, and cheA, in the endophytic microbiome of *A. konjac* roots significantly increased at 48 hpi or 96 hpi, whereas the changes in *A. muelleri* root tissues were less pronounced. After infection, the internal tissues of *A. konjac* petioles exhibited water-soaked rot, which spread upward and downward along the vascular bundle tissues, leading to disease symptoms in the root or leaf tissues. Therefore, it was reasonable for the chemotactic response of endophytic microbes in *A. konjac* roots to be stronger than that in *A. muelleri*. Furthermore, we found that microbial functional genes in the signal transduction mechanism module were enriched in the root tissues of both *Amorphophallus* species after infection, and the gene abundance of this module at both 48 hpi and 96 hpi was greater in *A. muelleri* than in *A. konjac*. These results suggest that the ability of endophytic microbes in the roots of both *Amorphophallus* species to perceive, transmit, and respond to signaling molecules was enhanced after *Pcc* infection, which would help activate defense signaling pathways, strengthen plant defense responses, and improve plant adaptability. Additionally, the greater abundance of microbial functional genes in the signal transduction mechanism module in the root tissues of the resistant species *A. muelleri* further indicates its unique advantage in plant–microbe interactions.

Conclusions

Our results revealed that infection by the necrotrophic bacterial pathogen *Pcc* induces changes in the endophytic microbial communities within different compartments of susceptible and resistant konjac, and bacterial communities are more sensitive to *Pcc* than are fungal communities. Under *Pcc* stress, the negative interactions within the bacterial-fungal interdomain network intensified, suggesting that endophytic fungal taxa in konjac may protect the host plant through ecological competition or by inhibiting pathogen growth. Compared with those of susceptible *A. konjac*, the microbial communities associated with the resistant species *A. muelleri* under *Pcc* stress presented unique advantages in enhancing adaptability to environmental changes, modulating plant immune signaling, strengthening plant cell walls, and inducing plant defense responses. This study deepens the understanding of the assembly and functional adaptive changes in endophytic microbial communities among konjac species with different resistance levels under necrotrophic bacterial pathogen stress, providing a theoretical basis for exploring and utilizing endophytic fungal resources in resistant konjac.

Methods

Inoculation experiment description and sampling

In this study, the inoculation experiment was conducted in the greenhouse of Yunnan Key Laboratory of Konjac Biology/Yunnan Urban Agricultural Engineering and Technological Research Center. The soft rot pathogen strain *P. carotovorum* subsp. *carotovorum* EccK-23B (accession number: MN653919) used in this study has been preserved in our laboratory. We selected two konjac species with different resistances: *A. konjac* and *A. muelleri*. Among them, *A. konjac* is highly susceptible to *Pcc*, whereas *A. muelleri* is highly resistant[1]. We planted one-year-old underground bulbs of the above two konjac species in the same greenhouse. We selected completely healthy *A. konjac* and *A. muelleri* plants that had been grown in the greenhouse for five months as experimental materials. One hundred microliters of *Pcc* bacterial culture (1×10^8 CFU/mL) was inoculated at a position 1–2 cm away from the leaf bifurcation on the upper part of the petiole, and inoculation was performed with an equal amount of sterile water as a control.

This experiment consisted of a total of 10 treatments. The treatments for *A. konjac* were as follows: before inoculation (H0), inoculation with sterile water for 48 h (H48), inoculation with sterile water for 96 h (H96), inoculation with *Pcc* for 48 h (D48), and inoculation with *Pcc* for 96 h (D96). The treatments for *A. muelleri* were as follows: before inoculation (H0), inoculation with sterile water for 48 h (H48), inoculation with sterile water for 96 h (H96), inoculation with *Pcc* for 48 h (D48), and inoculation with *Pcc* for 96 h (D96). Each treatment had 3 biological replicates, and each biological replicate involved a single konjac plant. Furthermore, to ensure disease

occurrence in konjac, we inoculated 6 konjac plants with *Pcc* for each treatment. At each sampling stage, 3 plants with relatively consistent infection symptoms or infection severity were selected for sampling.

When collecting samples, the whole plants from each treatment group were removed from the soil, and a large amount of sterile water was used to wash away the soil attached to the roots. The konjac plants were subsequently divided into three parts: roots, petioles, and leaves. To avoid contamination by environmental microorganisms, the cut tissue segments were rinsed with 75% ethanol for 30 s and 3% sodium hypochlorite solution for 3 min and then rinsed with sterilized distilled water 3 times for surface sterilization. After surface disinfection, a sterile scalpel was used to cut the tissue segments into small pieces of approximately 1 mm, and these segments were thoroughly mixed to be regarded as one sample. The well-mixed samples were placed in 10-ml sterile conical tubes, quickly frozen in liquid nitrogen and immediately stored in a −80 °C freezer until use. A total of 90 plant tissue samples were collected (90 samples = 10 treatments × 3 compartments × 3 biological replicates) and divided into 30 different sample groups. Details on sample collection and grouping are shown in Fig. 2a, while Supplementary Table 13 provides an expanded explanation of the group names.

Microbial DNA extraction and amplicon sequencing

Total DNA was extracted from the 90 tissue samples via the FastDNA® Spin Kit for Soil (MP Biomedicals, Solon, OH, USA) following the manufacturer's instructions. The DNA concentration and purity were examined using a NanoDrop 2000, and the DNA extraction quality was examined using 1% agarose gel electrophoresis. The endophytic fungal diversity was analyzed using the universal primers ITS1F and ITS2R. For the analysis of bacterial communities, two-step PCR amplification was performed, with the bacterial primers 799F/1392R[75] and 799F/1193R[76] used for 16S rRNA gene amplification. The PCR amplification conditions are shown in Supplementary Table 14. Amplicon libraries were sequenced on the Illumina HiSeq 2500 platform at Shanghai Majorbio Bio-Pharm Technology Co., Ltd.

Analysis of amplicon sequencing data

Usearch software[77] was used to filter the obtained sequences and remove chimeric sequences to obtain the valid sequences. After chimera removal, the processed high-quality sequencing reads were clustered into operational taxonomic units (OTUs) by Uparse software on the basis of 97% pairwise identity. Taxonomic assignment was performed using the SILVA reference database[78] and UNITE database[79] for bacteria and fungi, respectively. The bacterial OTUs assigned to the chloroplast, mitochondrion, or Viridiplantae, as well as the fungal OTUs that were assigned to plants or protists, were removed. In total, 3,586,354 effective bacterial sequences and 4,168,174 effective fungal sequences were recorded from the 90 plant samples, with average lengths of 375 bp and 225 bp, respectively. Taxonomic annotation was performed on the valid reads at the 97% sequence similarity level, and a total of 2349 bacterial and 2354 fungal OTUs were recovered from all 90 samples. Mothur was used to generate rarefaction curves; calculate the library coverage; calculate the Shannon and Chao1 indices; and evaluate the species alpha diversity indices. Bray–Curtis dissimilarity metrics were calculated and visualized via nonmetric multidimensional scaling (NMDS) ordinations to assess the beta diversity of the bacterial and fungal communities. To minimize the effects of sequencing depth on alpha and beta diversity, the number of 16S rRNA gene and ITS sequences from each sample was rarefied to 20,891 and 30,095, respectively (Supplementary Fig. 10).

Isolation of endophytic microorganisms from *Amorphophallus* spp. and evaluation of their antagonistic effects on the soft rot pathogen (*Pcc*)

Isolation and purification: In accordance with the methods described in section 1.2 of this study, we sterilized the surfaces of the tissue segments. After the surface moisture was absorbed with sterile filter paper, the tissue was cut into 0.5 cm × 0.5 cm pieces with a sterile dissecting knife. The tissue pieces were placed on preprepared rose bengal agar and nutrient agar, with 3–5 pieces per dish. The dishes were incubated at 28 ± 1 °C for 7 days. The colonies obtained were subcultured on potato dextrose agar (PDA) until pure cultures were obtained.

Preparation of test strains: The isolated endophytic bacterial strains and the phytopathogen were inoculated into LB broth, shaken overnight, and then diluted with sterile distilled water to a seeding concentration of 1×10^8 CFU/mL. The isolated endophytic fungal strains were cultured on PDA medium and incubated for 7 days before examination of the antagonism. Then, a 5-mm-diameter colony cake was punched out for use.

Antagonism test: For this test, 200 μL of *Pcc* bacterial culture was evenly coated on PDA medium, and 25 μL of the isolated bacterial culture was inoculated in the center of the plate. For the screening of fungal strains, the prepared test fungus cake was placed face down on the PDA plate. Each treatment was repeated three times. After inoculation, the diameters of the inhibition zone and colonies were measured by the cross method at 28°C for 24 h.

Identification of antagonistic fungi: The fungal genomic DNA was extracted using the modified CTAB method. The internal transcribed spacer (ITS) region was amplified via the primer pair ITS1/ITS4[80]. The PCR amplification conditions are shown in Supplementary Table 14. Sanger sequencing was performed with the same primers used for PCR by Qingke Biotechnology Co., Ltd. (Beijing, China). All fungal isolates were identified through BLAST searches against the NCBI database with ITS sequences.

Metagenomic sequencing workflow and data analysis

To further characterize the *A. konjac* and *A. muelleri* microbiome functions under *Pcc* stress, we selected 18 root and 18 petiole DNA samples from these two species for metagenomic sequencing. Thirty-six DNA samples were sequenced via an Illumina NovaSeq 6000 instrument with a paired-end protocol (Illumina Inc., San Diego, CA, USA) at Majorbio Bio-Pharm Technology Co., Ltd. (Shanghai, China). The raw sequences were quality-filtered using Fastp[81] (v0.23.0), and the sequences belonging to the *A. konjac* and *A. muelleri* genomes were removed by mapping the data to the *A. konjac* (genome assembly sequence accession number: PRJNA734512) and *A. muelleri* reference genomes with BWA (v0.7.17). Finally, an average of 88,109,758 clean reads was retrieved for each DNA sample.

The remaining reads were assembled by using MEGAHIT[82] (v1.1.2), predicted on the basis of contigs via Prodigal[83] (v2.6.3), and clustered with 90% sequence identity and 90% coverage by using CD-HIT[84] (v4.6.1) to generate a nonredundant gene catalog. High-quality reads were aligned to nonredundant gene catalogs to calculate gene abundance with 95% identity using SOAPaligner[85]. Representative sequences of the nonredundant gene catalog were aligned to the NR database (v20230830) with an e-value cutoff of $1e^{-5}$ using Diamond[86] (v2.0.13) for taxonomic annotations. The KEGG annotation and cluster of orthologous groups of proteins (COG) annotation for the representative sequences were performed using Diamond (v2.0.13) against the Kyoto Encyclopedia of Genes and Genomes database (v20230830) and COG database (v2020), with an e-value cutoff of $1e^{-5}$. Carbohydrate-active enzyme annotation was conducted using hmmscan against the CAZy database (v12) with an e-value cutoff of $1e^{-5}$. A nonparametric statistical test (Kruskal–Wallis test) was performed to evaluate differences in functions or gene abundance among different groups.

Statistics and reproducibility

Bioinformatic analyses of the amplicon and metagenomic sequencing data were conducted on the Majorbio Cloud platform (https://cloud.majorbio.com). For amplicon sequencing data, rarefaction curves and alpha diversity indices (Chao1 and Shannon) were calculated using Mothur. Intergroup differences in alpha diversity were assessed via Wilcoxon rank-sum tests. Bray–Curtis dissimilarity metrics were calculated and visualized via nonmetric multidimensional scaling (NMDS) ordinations to assess the beta diversity of the bacterial and fungal communities. Permutational multivariate analysis of variance (PERMANOVA) statistical tests were performed to determine the effects of different factors on community dissimilarity using "adonis" in the vegan R package[87]. Co-occurrence networks of bacterial and fungal communities were constructed using the SparCC method

(correlation threshold: $|r| > 0.75$, $P < 0.05$) via the integrated network analysis pipeline (iNAP, https://github.com/yedeng-lab/iNAP)[88], followed by visualization in Gephi[89]. Kruskal-Wallis or Wilcoxon rank-sum tests were applied to identify significant differences in the relative abundance of microbial taxa or functional genes/modules across sample groups. Intergroup variations in Shannon and Chao diversity indices of KO, COG, and CAZy functional profiles were assessed using Duncan's multiple range test ($\alpha = 0.05$, IBM SPSS Statistics 18.0). All inoculation experiments in this study were performed with three independent biological replicates. Each replicate was defined as the inoculation of one individual konjac plant. Statistical analyses were based on a sample size of $n = 3$ per group.

Reporting summary

Further information on research design is available in the Nature Portfolio Reporting Summary linked to this article.

Data availability

The raw sequencing data have been deposited in the NCBI Sequence Read Archive (SRA) database under the accession numbers PRJNA1051780 and PRJNA1051810 (amplicon) and PRJNA1053770, PRJNA1054065, PRJNA1054692, and PRJNA1055190 (metagenomic). All source data underlying the graphs presented in the main figures of this study can be found in the supplementary materials under [Supplementary Data 1-6]. All other data are available from the corresponding author on reasonable request.

Code availability

The data analysis in this study was conducted on the Majorbio Cloud Platform (www.majorbio.com) without using custom code.

Received: 23 July 2024; Accepted: 7 May 2025;
Published online: 19 May 2025

References

1. Wei, H. et al. Comparative physiological and transcriptomic profiles reveal regulatory mechanisms of soft rot disease resistance in *Amorphophallus* spp. *Physiol. Mol. Plant Pathol.* **118**, 101807 (2022).
2. Yang, M. et al. Different response mechanisms of rhizosphere microbial communities in two species of *Amorphophallus* to *Pectobacterium carotovorum* subsp. *carotovorum* infection. *Plant Pathol. J.* **39**, 207–219 (2023).
3. Gao, P. H. et al. Weighted gene coexpression analysis network-based analysis of candidate pathways and hub genes in konjac soft rot-resistance. *J. Am. Soc. Hort. Sci.* **147**, 322333 (2022).
4. Czajkowski, R., PÃ©rombelon, M. C. M., van Veen, J. A. & Van der Wolf, J. M. Control of blackleg and tuber soft rot of potato caused by *Pectobacterium* and *Dickeya* species: a review. *Plant Pathol.* **60**, 999–1013 (2011).
5. Davidsson, P. R., Kariola, T., Niemi, O. & Palva, E. T. Pathogenicity of and plant immunity to soft rot pectobacteria. *Front. Plant Sci.* **4**, 191 (2013).
6. Toth, I. K., Bell, K. S., Holeva, M. C. & Birch, P. R. Soft rot erwiniae: from genes to genomes. *Mol. Plant Pathol.* **4**, 17–30 (2003).
7. Ma, B. et al. Host range and molecular phylogenies of the soft rot enterobacterial genera *Pectobacterium* and *Dickeya*. *Phytopathology* **97**, 1150–1163 (2007).
8. Mansfield, J. et al. Top 10 plant pathogenic bacteria in molecular plant pathology. *Mol. Plant Pathol.* **13**, 614–629 (2012).
9. Chan, Y. C., Wu, H. P. & Chang, D. Y. Extracellular secretion of carocin S1 in *Pectobacterium carotovorum* subsp. *carotovorum* occurs via the type III secretion system integral to the bacterial flagellum. *BMC Microbiol.* **9**, 181–190 (2009).
10. Chang, C. P. et al. Unleashing the influence of cAMP receptor protein: the master switch of bacteriocin export in *Pectobacterium carotovorum* subsp. *carotovorum*. *Int. J. Mol. Sci.* **24**, 9752 (2023).
11. Trivedi, P., Leach, J. E., Tringe, S. G., Sa, T. & Singh, B. K. Plant-microbiome interactions: from community assembly to plant health. *Nat. Rev. Microbiol.* **18**, 607–621 (2020).
12. Martin, F. M., Uroz, S. & Barker, D. G. Ancestral alliances: plant mutualistic symbioses with fungi and bacteria. *Science* **356**, eaad4501 (2017).
13. Turner, T. R., James, E. K. & Poole, P. S. The plant microbiome. *Genome Biol.* **14**, 209 (2013).
14. Simon, J. C., Marchesi, J. R., Mougel, C. & Selosse, M. A. Host-microbiota interactions: from holobiont theory to analysis. *Microbiome* **7**, 5 (2019).
15. Vandenkoornhuyse, P., Quaiser, A., Duhamel, M., Le Van, A. & Dufresne, A. The importance of the microbiome of the plant holobiont. *N. Phytol.* **206**, 1196–1206 (2015).
16. Mendes, R. et al. Deciphering the rhizosphere microbiome for disease-suppressive bacteria. *Science* **332**, 1097–1100 (2011).
17. Hassani, M. A., Duran, P. & Hacquard, S. Microbial interactions within the plant holobiont. *Microbiome* **6**, 58 (2018).
18. Sessitsch, A., Pfaffenbichler, N. & Mitter, B. Microbiome applications from lab to field: facing complexity. *Trends Plant Sci.* **24**, 194–198 (2019).
19. Larousse, M. et al. Tomato root microbiota and *Phytophthora parasitica*-associated disease. *Microbiome* **5**, 56 (2017).
20. Li, P. D. et al. The phyllosphere microbiome shifts toward combating melanose pathogen. *Microbiome* **10**, 56 (2022).
21. Li, Y. et al. Microbiota and functional analyses of nitrogen-fixing bacteria in root-knot nematode parasitism of plants. *Microbiome* **11**, 48 (2023).
22. Berendsen, R. L. et al. Disease-induced assemblage of a plant-beneficial bacterial consortium. *ISME J.* **12**, 1496–1507 (2018).
23. Shi, W. et al. The occurrence of potato common scab correlates with the community composition and function of the geocaulosphere soil microbiome. *Microbiome* **7**, 14 (2019).
24. Adams, A. S. et al. Cellulose-degrading bacteria associated with the invasive wood-wasp Sirex noctilio. *ISME J.* **5**, 1323–1331 (2011).
25. Manna, M. & Seo, Y. S. Plants under the attack of allies: moving towards the plant pathobiome paradigm. *Plants* **10**, 125 (2021).
26. Cordovez, V., Dini-Andreote, F., Carrión, V. J. & Raaijmakers, J. M. Ecology and evolution of plant microbiomes. *Annu. Rev. Microbiol.* **73**, 69–88 (2019).
27. Yin, C. et al. Rhizosphere community selection reveals bacteria associated with reduced root disease. *Microbiome* **9**, 1–18 (2021).
28. Liu, H. et al. Evidence for the plant recruitment of beneficial microbes to suppress soil-borne pathogens. *N. Phytol.* **229**, 2873–2885 (2021).
29. Toju, H. et al. Core microbiomes for sustainable agroecosystems. *Nat. Plants* **4**, 247–257 (2018).
30. Pandey, S. S. et al. Plant probiotics - endophytes pivotal to plant health. *Microbiol. Res.* **263**, 127148 (2022).
31. Laforest-Lapointe, I., Paquette, A., Messier, C. & Kembel, S. W. Leaf bacterial diversity mediates plant diversity and ecosystem function relationships. *Nature* **546**, 145–147 (2017).
32. Remus-Emsermann, M. N. P. & Schlechter, R. O. Phyllosphere microbiology: at the interface between microbial individuals and the plant host. *N. Phytol.* **218**, 1327–1333 (2018).
33. Zhou, X. et al. Cross-kingdom synthetic microbiota supports tomato suppression of *Fusarium* wilt disease. *Nat. Commun.* **13**, 7890 (2022).
34. Lee, S. M., Kong, H. G., Song, G. C. & Ryu, C. M. Disruption of Firmicutes and Actinobacteria abundance in tomato rhizosphere causes the incidence of bacterial wilt disease. *ISME J.* **15**, 330–347 (2021).
35. Wen, T. et al. Specific metabolites drive the deterministic assembly of diseased rhizosphere microbiome through weakening microbial degradation of autotoxin. *Microbiome* **10**, 177 (2022).
36. Gao, M. et al. Disease-induced changes in plant microbiome assembly and functional adaptation. *Microbiome* **9**, 187 (2021).

37. Zhang, Z., Li, J., Zhang, Z., Liu, Y. & Wei, Y. Tomato Endophytic bacteria composition and mechanism of suppressiveness of wilt disease (*Fusarium oxysporum*). *Front. Microbiol.* **12**, 731764 (2021).
38. Tan, L. et al. Network analysis reveals the root endophytic fungi associated with *Fusarium* root rot invasion. *Appl. Soil Ecol.* **78**, 104567 (2022).
39. Carrión, V. J. et al. Pathogen-induced activation of disease-suppressive functions in the endophytic root microbiome. *Science* **366**, 606–612 (2019).
40. Matsumoto, H. et al. Bacterial seed endophyte shapes disease resistance in rice. *Nat. Plants* **7**, 60–72 (2021).
41. Stringlis, I. A. et al. MYB72-dependent coumarin exudation shapes root microbiome assembly to promote plant health. *Proc. Natl Acad. Sci. USA* **115**, E5213–E5222 (2018).
42. Zhalnina, K. et al. Dynamic root exudate chemistry and microbial substrate preferences drive patterns in rhizosphere microbial community assembly. *Nat. Microbiol.* **3**, 470–480 (2018).
43. Ding, T. & Melcher, U. Influences of plant species, season and location on leaf endophytic bacterial communities of non-cultivated plants. *PLoS One* **11**, e0150895 (2016).
44. Yang, M. et al. The endophytic fungal community plays a crucial role in the resistance of host plants to necrotic bacterial pathogens. *Physiol. Plant.* **176**, e14284 (2024).
45. He, F. Response of root-associated bacterial communities to different degrees of soft rot damage in *Amorphophallus konjac* under a *Robinia pseudoacacia* plantation. *Front. Microbiol.* **12**, 652758 (2021).
46. Gu, Y. et al. Small changes in rhizosphere microbiome composition predict disease outcomes earlier than pathogen density variations. *ISME J.* **16**, 2448–2456 (2022).
47. Cregger, M. A. et al. The Populus holobiont: dissecting the effects of plant niches and genotype on the microbiome. *Microbiome* **6**, 31 (2018).
48. Kwak, M. J. et al. Rhizosphere microbiome structure alters to enable wilt resistance in tomato. *Nat. Biotechnol.* **36**, 1100–1109 (2018).
49. Seybold, H. et al. A fungal pathogen induces systemic susceptibility and systemic shifts in wheat metabolome and microbiome composition. *Nat. Commun.* **11**, 1910 (2020).
50. Charkowski, A. et al. The role of secretion systems and small molecules in soft-rot enterobacteriaceae pathogenicity. *Annu. Rev. Phytopathol.* **50**, 425–449 (2012).
51. Antúnez-Lamas, M. et al. Role of motility and chemotaxis in the pathogenesis of Dickeya dadantii 3937 (ex *Erwinia chrysanthemi* 3937). *Microbiology* **155**, 434–442 (2009).
52. O'Toole, R., Milton, D. L. & Wolf-Watz, H. Chemotactic motility is required for invasion of the host by the fish pathogen *Vibrio anguillarum*. *Mol. Microbiol.* **19**, 625–637 (1996).
53. Tanui, C. K., Shyntumm D, Y., Sedibane, P. K., Bellieny-Rabelo, D. & Moleleki, L. N. *Pectobacterium brasiliense* 1692 chemotactic responses and the role of methyl-accepting chemotactic proteins in ecological fitness. *Front. Plant Sci.* **12**, 650894 (2021).
54. Glasner, J. D. et al. Niche-specificity and the variable fraction of the *Pectobacterium* pan-genome. *Mol. Plant Microbe Interact.* **21**, 1549–1560 (2008).
55. Moulton, R. C. & Montie, T. C. Chemotaxis by *Pseudomonas aeruginosa*. *J. Bacteriol.* **137**, 274–280 (1979).
56. Sampedro, I., Parales, R. E., Krell, T. & Hill, J. E. *Pseudomonas chemotaxis*. *FEMS Microbiol. Rev.* **39**, 17–46 (2015).
57. Garrity, L. F. & Ordal, G. W. Chemotaxis in *Bacillus subtilis*: How bacteria monitor environmental signals. *Pharmacol. Ther.* **68**, 87–104 (1995).
58. Agler, M. T. et al. Microbial hub taxa link host and abiotic factors to plant microbiome variation. *PLoS Biol.* **14**, e1002352 (2016).
59. Coyte, K. Z., Schluter, J. & Foster, K. R. The ecology of the microbiome: networks, competition, and stability. *Science* **350**, 663–666 (2015).
60. Wagg, C., Schlaeppi, K., Banerjee, S., Kuramae, E. E. & van der Heijden, M. G. A. Fungal-bacterial diversity and microbiome complexity predict ecosystem functioning. *Nat. Commun.* **10**, 4841 (2019).
61. Wang, Y., Zhang, S. & Chen, G. Construction of an engineered Saccharomyces cerevisiae expressing endoglucanase efficiently. *Sheng Wu Gong. Cheng Xue Bao.* **36**, 2193–2205 (2020). (in Chinese).
62. Lei, L. R. et al. Research advances in the structures and biological activities of secondary metabolites from *Talaromyces*. *Front. Microbiol.* **13**, 984801 (2022).
63. Chen, X. L. et al. Effects of *Meloidogyne incognita* on the fungal community in tobacco rhizosphere. *Rev. Bras. Cienc. Solo.* **46**, e0210127 (2022).
64. Astudillo-García, C. et al. Evaluating the core microbiota in complex communities: a systematic investigation. *Environ. Microbiol.* **19**, 1450–1462 (2017).
65. Lemanceau, P., Blouin, M., Muller, D. & Moënne-Loccoz, Y. Let the core microbiota be functional. *Trends Plant Sci.* **22**, 583–595 (2017).
66. Yeoh, Y. K. et al. Evolutionary conservation of a core root microbiome across plant phyla along a tropical soil chronosequence. *Nat. Commun.* **8**, 215 (2017).
67. Rumiana V. R. Chapter 2 - Effects of pathogens and disease on plant physiology. In: Richard P. editor. Oliver, Agrios' Plant Pathology, 6th ed. 63–92, Academic Press; London, UK; 2024.
68. Zhang, W. et al. Adaptation of intertidal biofilm communities is driven by metal ion and oxidative stresses. *Sci. Rep.* **3**, 3180 (2013).
69. Negi, N. P. et al. The calcium connection: exploring the intricacies of calcium signaling in plant-microbe interactions. *Front. Plant Sci.* **14**, 1248648 (2023).
70. Delmer, D., Dixon, R. A., Keegstra, K. & Mohnen, D. The plant cell wall–dynamic, strong, and adaptable–is a natural shapeshifter. *Plant Cell.* **36**, 1257–1311 (2024).
71. Molina, A. et al. Plant cell walls: source of carbohydrate-based signals in plant-pathogen interactions. *Curr. Opin. Plant Biol.* **82**, 102630 (2024).
72. de Vries, S. & de Vries, J. A global survey of carbohydrate esterase families 1 and 10 in Oomycetes. *Front. Genet.* **11**, 756 (2020).
73. Nakamura, A. M., Nascimento, A. S. & Polikarpov, I. Structural diversity of carbohydrate esterases. *Biotechnol. Res. Innov.* **1**, 35–51 (2017).
74. Li, X. et al. Functional validation of two fungal subfamilies in carbohydrate esterase family 1 by biochemical characterization of esterases from uncharacterized branches. *Front. Bioeng. Biotechnol.* **8**, 694 (2020).
75. Hanshew, A. S., Mason, C. J., Raffa, K. F. & Currie, C. R. Minimization of chloroplast contamination in 16S rRNA gene pyrosequencing of insect herbivore bacterial communities. *J. Microbiol. Methods* **95**, 149–155 (2013).
76. Bulgarelli, D. et al. Revealing structure and assembly cues for *Arabidopsis* root-inhabiting bacterial microbiota. *Nature* **488**, 91–95 (2012).
77. Edgar, R. C. UPARSE: highly accurate OTU sequences from microbial amplicon reads. *Nat. Methods* **10**, 996–998 (2013).
78. Quast, C. et al. The SILVA ribosomal RNA gene database project: improved data processing and web-based tools. *Nucleic Acids Res.* **41**, D590–D596 (2013).
79. Kõljalg, U. et al. UNITE: a database providing web-based methods for the molecular identification of ectomycorrhizal fungi. *N. Phytol.* **166**, 1063–1068 (2005).
80. Nilsson, R. H. et al. Mycobiome diversity: high-throughput sequencing and identification of fungi. *Nat. Rev. Microbiol.* **17**, 95–109 (2019).
81. Chen, S., Zhou, Y., Chen, Y. & Gu, J. fastp: an ultra-fast all-in-one FASTQ preprocessor. *Bioinformatics* **34**, i884–i890 (2018).

82. Li, D., Liu, C. M., Luo, R., Sadakane, K. & Lam, T. W. MEGAHIT: an ultra-fast single-node solution for large and complex metagenomics assembly via succinct de Bruijn graph. *Bioinformatics* **31**, 1674–1676 (2015).
83. Hyatt, D. et al. Prodigal: prokaryotic gene recognition and translation initiation site identification. *BMC Bioinforma.* **11**, 119–119 (2010).
84. Fu, L., Niu, B., Zhu, Z., Wu, S. & Li, W. CD-HIT: accelerated for clustering the next-generation sequencing data. *Bioinformatics* **28**, 3150–3152 (2012).
85. Li, R., Li, Y., Kristiansen, K. & Wang, J. SOAP: short oligonucleotide alignment program. *Bioinformatics* **24**, 713–714 (2008).
86. Buchfink, B., Xie, C. & Huson, D. H. Fast and sensitive protein alignment using DIAMOND. *Nat. Methods* **12**, 59–60 (2015).
87. Oksanen, J. et al. The vegan package. *Comm. Ecol. Pack.* **10**, 631–637 (2007).
88. Feng, K. et al. iNAP: an integrated network analysis pipeline for microbiome studies. *iMeta* **1**, e13 (2022).
89. Bastian, M., Heymann, S. & Jacomy, M. Gephi: an open source software for exploring and manipulating networks. *ICWSM* **3**, 361–362 (2009).

Acknowledgements

This study was funded by Yunnan Provincial Science and Technology Department (grant no. 202501AU070008, 202449CE340009, 202201AU070043, 202101BA070001-174); Yunnan Education Department Research Project (grant no. 2025J0753, 2023J0827); Talent Introduction Program of Kunming University (No. YJL24014) and Yunnan Province Yu Lei Expert Grassroots Research Workstation (grant no. 20231023-135).

Author contributions

L.Y. and M.Y. conceived and designed the experiments; M.Y. analyzed the amplicon/metagenomic data and wrote and edited the article; Y.Q. and P.H.G. performed the experiments and collected the samples; M.Y., J.W.G. and L.F.L. conducted the laboratory experiments and isolated and identified the antagonistic fungal strains. Y.T.Z. and J.N.L. contributed to drawing; Y.T.Z., Z.B.C. and L.Y. contributed to the revision of the manuscript.

Competing interests

The authors declare no competing interests.

Additional information

Supplementary information The online version contains supplementary material available at https://doi.org/10.1038/s42003-025-08196-4.

Correspondence and requests for materials should be addressed to Lei Yu.

Peer review information *Communications Biology* thanks Vitor Heidrich and the other, anonymous, reviewers for their contribution to the peer review of this work. Primary Handling Editor: David Favero.